An auxiliary strategy of partial least squares regression in pharmacokinetic/pharmacodynamic studies: A case of application of guhong injection in myocardial ischemia/reperfusion rats

Recommended Citation
Chen, Hai-yang; Li, Chang; Shao, Chong-yu; Wu, Yu-jia; Wan, Hai-tong; and He, Yu (2024) "An auxiliary strategy of partial least squares regression in pharmacokinetic/pharmacodynamic studies: A case of application of guhong injection in myocardial ischemia/reperfusion rats," *Journal of Food and Drug Analysis*: Vol. 32 : Iss. 1 , Article 6.
Available at: https://doi.org/10.38212/2224-6614.3492

An auxiliary strategy of partial least squares regression in pharmacokinetic/pharmacodynamic studies: A case of application of guhong injection in myocardial ischemia/reperfusion rats

Hai-yang Chen [a], Chang Li [b], Chong-yu Shao [b], Yu-jia Wu [b], Hai-tong Wan [b,*], Yu He [a,**]

[a] School of Pharmaceutical Sciences, Zhejiang Chinese Medical University, Hangzhou, 310053 Zhejiang, China
[b] School of Basic Medical Sciences, Zhejiang Chinese Medical University, Hangzhou, 310053 Zhejiang, China

Abstract

Guhong injection (GHI) has been applied in the therapy of cardio-cerebrovascular disease in clinic, but there is no report about the pharmacokinetic/pharmacodynamic (PK/PD) research on GHI treating myocardial ischemia/reperfusion (MI/R) injury in rats. In this study, eight compounds of GHI in plasma, including N-acetyl-L-glutamine (NAG), chlorogenic acid (CGA), hydroxysafflor yellow A (HSYA), p-coumaric acid (pCA), rutin, hyperoside, kaempferol-3-O-rutinoside, and kaempferol-3-O-glucoside, were quantified by LC-MS/MS. We discovered that the values of $t_{1/2\beta}$, k_{12}, V_2, and CL_2 were larger than those of $t_{1/2\alpha}$, k_{21}, V_1, and CL_1 for all compounds. The levels of four biomarkers, creatine kinase-MB (CK-MB), cardiac troponin I (cTn I), ischemia-modified albumin (IMA), and alpha-hydroxybutyrate dehydrogenase (α-HBDH) in plasma were determined by ELISA. The elevated level of these biomarkers induced by MI/R was declined to different degrees via administrating GHI and verapamil hydrochloride (positive control). The weighted regression coefficients of NAG, HSYA, CGA, and pCA in PLSR equations generated from The Unscrambler X software (version 11) were mostly minus, suggesting these four ingredients were positively correlated to the diminution of the level of four biomarkers. E_{max} and ED_{50}, two parameters in PK/PD equations that were obtained by adopting Drug and Statistics software (version 3.2.6), were almost enlarged with the rise of GHI dosage. Obviously, all analytes were dominantly distributed and eliminated in the peripheral compartment with features of rapid distribution and slow elimination. With the enhancement of GHI dosage, the ingredients only filled in the central compartment if the peripheral compartment was replete. Meanwhile, high-dose of GHI generated the optimum intrinsic activity, but the affinity of compounds with receptors was the worst, which may be caused by the saturation of receptors. Among the eight analytes, NAG, HSYA, CGA, and pCA exhibited superior cardioprotection, which probably served as the pharmacodynamic substance basis of GHI in treating MI/R injury.

Keywords: Guhong injection, Myocardial ischemia/reperfusion, Pharmacokinetic/pharmacodynamic model, Partial least squares regression

1. Introduction

Acute myocardial infarction (AMI), one cardiovascular disease accompanied by high morbidity and mortality, is clinically manifested as the ischemic necrosis of the local myocardium induced by the acute occlusion of coronary arteries and the interruption of blood flow [1]. The dominant therapy of AMI, percutaneous coronary intervention, has been proposed as early as the last century and extended to nowadays [2,3]. Although percutaneous coronary intervention surgery has made great progress in treating AMI, it inevitably brought secondary damage to myocardial tissue due to the sudden restoration of blood, which was known as myocardial ischemia/reperfusion (MI/R) injury. The pathomechanisms of MI/R injury were diversiform and mutually interacted, mainly including oxidative stress, inflammatory response, calcium overload, energy metabolism retardation, as well as the modulation of endothelin and angiotensin. Chinese herbal medicine, owing to its character of multi-ingredients and multi-targets, may accomplish great deeds when facing so involute pathogenesis of MI/R injury. For instance, hydroxysafflor yellow A (HSYA) and carthamin yellow, two active ingredients segregated from safflower (*Carthamus tinctorius* L.), were confirmed to extenuate MI/R injury via mitigating both oxidative stress and inflammation [4–6]. It follows that Chinese herbal medicine, one indispensable part of world medicine, also manifests gigantic potentiality in treating MI/R injury.

The pharmacokinetic/pharmacodynamic (PK/PD) modeling regards the time axis as one shared independent variable to study the affiliation of drug concentration and curative effect [7]. The information generated from unilateral PK or PD research is incomplete and insufficient and is not able to amply elucidate the process of drugs *in vivo*. The single PK research is to investigate the disposal (i.e., absorption, distribution, metabolism, and excretion) of drugs by an organism via monitoring the concentration of drugs to construct the time–concentration curve, but the change of concentrations that are intently related to the curative effect is more valuable to study [8]. The single PD study only provides the dynamic process for the impact of drugs on an organism over time, but it is uncertain whether this influence will be maximized when the drug concentration reaches to peak in plasma [9]. Therefore, it is necessary to establish a PK/PD binding model to estimate the concentration–time–effect relation of drugs to explore the correlation between the concentration and efficacy of drugs in the target sites, thereby evaluating the process of drugs *in vivo*.

Partial least squares regression (PLSR), a machine learning approach that combines the merit of principal component analysis, canonical correlation analysis, and multiple linear regression analysis, is extensively adopted to investigate the correlation of multiple dependent variables with an independent variable through the combination of dimensionality reduction and linear regression [10]. In the former studies, PLSR has been constantly employed in exploring the spectrum–effect relationship to determine predominant therapeutic components of compound preparations in light of whether the regression coefficient in equations was plus or minus [11–13]. In the current study, PLSR was first applied to investigate the correlation between PK indicators and PD indexes.

Creatine kinase-MB (CK-MB), an isozyme of creatine kinase that predominantly resides in the myocardium, belongs to one indicator that is sensitive to myocardial tissue injury [14]. The formation of ischemia-modified albumin (IMA) was retraced to the destruction of the amino acid sequence of albumin by massive free radicals produced in oxidative stress response, leading to the alteration of its binding ability with transition metals [15]. IMA was extensively chosen as one biomarker to diagnose myocardial ischemia accompanied by the oxidative stress response [16,17]. Cardiac troponin I (cTn I), one gold standard for the determination of myocardial ischemia, is extremely specific and sensitive to the diminutive myocardial injury, and effectively avoided the false positive of CK-MB caused by skeletal muscle damage in the clinic [18,19]. Alpha-hydroxybutyrate dehydrogenase (α-HBDH), as the type I isoenzyme of lactic dehydrogenase, dominantly exists in myocardial tissues, and serves as one of the monumental biomarkers of cardiac diseases [19,20]. Taken together, these four myocardial enzymes that were usually adopted for clinical diagnosis of MI/R were selected as the PD indicators by us to investigate the cardioprotection of guhong injection (GHI).

Although GHI, composed of N-acetyl-L-glutamine (NAG) and the aqueous extract of safflower (*C. tinctorius* L.), has been attested to mitigate MI/R injury via improving oxidative stress to inhibit apoptosis by our previous study, the specific process of GHI *in vivo* is not revealed plenty [21]. Although our team explored the PK parameters of only two active ingredients of GHI in both cerebral ischemia/reperfusion rats and normal rats, we deemed that this research was incomplete [22]. Hence, in this

paper, we aimed at integrating eight active compounds with four myocardial enzymes to investigate the PK/PD character of GHI when treating MI/R rats to furnish guidance for clinical medication. Meanwhile, the PLSR approach was yet adopted in our current study to additionally promulgate the effective substances and underlining mechanisms of GHI on the therapy of MI/R injury.

2. Materials and methods

2.1. Reagents and chemicals

The compound preparation, GHI, was provided by Buchang Company (batch number: 20220303, Shandong, China). The standards of chlorogenic acid (CGA, purity ≥98%, lot no. C10245363) and NAG (purity ≥99%, lot no. CMX769) were obtained from Shanghai Macklin Biochemical Co., Ltd (Shanghai, China); Kaempferol-3-O-rutinoside (K-3-R, purity ≥98%, lot no. 21070121) was supplied by Shanghai Tauto Biotech Co., Ltd (Shanghai, China); HSYA (purity ≥98%, lot no. DSTDQO001702) was obtained from Chengdu Desite Bio-Technology Co., Ltd (Sichuan, China); P-Coumaric acid (pCA, purity ≥99%, lot no. H-34002) was bought from Tianjin Heowns Biochem LLC (Tianjing, China); Rutin (RT, purity ≥98%, lot no. 0080−9705) was supplied by National Institute for the Control of Pharmaceutical and Biological Products (China); Verapamil hydrochloride (purity ≥99%, lot no. CMX769) and N-carbamoyl-L-glutamate (NCG, used as IS of NAG, purity ≥97%, lot no. BQY693) were offered from Shanghai Bide Pharmatech Ltd (Shanghai, China); Hyperoside (HYP, purity ≥98%, lot no. AF21031412), kaempferol-3-O-glucoside (K-3-G, purity ≥98%, lot no. AF20063001), and icariin (employed as internal standard of the other seven compounds, purity ≥98%, lot no. AF20102051) were purchased from Chengdu Alfa Biotechnology Co., Ltd (Sichuan, China). ELISA kits of CK-MB (lot no. 202010), IMA (lot no. 202210), cTn I (lot no. 202210), and α-HBDH (lot no. 202210) were bought from Meibiao Biology (Nanjing, China).

2.2. Animals and formation of MI/R model

The animal subjects, adult male Sprague Dawley rats (320−340g), were acquired from Shanghai B&K Experimental Animal Co., Ltd. (Shanghai, China) with production license: SCXK 2018−0006. They were reared in a specific pathogen-free sounding under approximately 50% humidity and 22 °C in Zhejiang Chinese Medical University Laboratory Animal Research Center (Laboratory animal use license: SYXK 2021−0012) with registration number of experimental animals: 20220411−04. The MI/R surgery in this article was consulted from our previous research [21]. In a nutshell, rats were firstly anesthetized by sodium pentobarbital (50 mg/kg, i.p.), and then were connected to a ventilator to guarantee normal breath, and their thoracic cavity was opened to emerge the heart. A 6.0 nylon thread was adopted to ligate the left anterior descending (LAD) for 30 min to establish myocardial ischemia, and the nylon thread was subsequently slackened for 1 h to accomplish reperfusion.

2.3. Experiment protocol

After one week adoption period, all rats were stochastically partitioned into six groups, as follows, sham group, model group, low-dose of GHI (GHI-L) group, middle-dose of GHI (GHI-M) group, high-dose of GHI (GHI-H) group, and verapamil hydrochloride group (VH, positive control). On the day before surgery, all rats were prohibited to forage but freely accessed to drink water. All rats in the sham group suffered from the sham operation, that is rats' heart was merely penetrated by the nylon thread but without LAD ligation. After the sham operation, rats were injected with physiological saline (10 mL/kg) through the tail vein. Apart from the rats in the sham group, all the others were subjected to surgery with ligating LAD. After the operation, rats in the model group were intravenously treated with physiological saline (10 mL/kg), GHI-administered groups were respectively injected with GHI (2.5, 5, and 10 mL/kg, i.v.), as well as in verapamil hydrochloride group was administered with verapamil hydrochloride (0.95 mg/kg) dissolved in physiological saline via tail vein. The administrated dosages of GHI and positive drug were converted from the clinical doses [21,23].

2.4. Plasma samples collection and distribution

After physiological saline, GHI or verapamil hydrochloride was respectively injected, approximate 400 μL blood was collected from the retro-orbital venous plexus of each rat at diverse time points (i.e., 2, 5, 10, 20, 40, 60, 90, 120, 240 and 360 min) into a 1.5 mL centrifuge tube with heparin sodium. All blood samples were left to rest for 30 min, and then centrifuged at 3500 rpm for 10 min at 4 °C. The plasma was gathered and dispensed to three new centrifuge tubes for storage at −80 °C, in which 100 μL and 20 μL for PK research and 50 μL for PD studies, respectively.

2.5. Quantitative analysis of eight analytes in GHI

To quantify eight analytes, 0.1 mL GHI was precisely suctioned and moved into a 20 mL volumetric flask, and then was diluted to tick mark by methanol−water solution (50:50, v/v). The diluted solution that was filtrated by filter membrane of 0.22 μm was employed for quantification of eight analytes with the help of LC-MS/MS. The adopted LC-MS/MS conditions and the final concentration of ISs were the same as the following described in the section of "pharmacokinetic research".

2.6. Pharmacokinetic research

2.6.1. LC-MS/MS apparatuses and conditions

The analytes in plasma for the PK study were quantified by engaging a LC-MS/MS system composited of DGU-20A5R(C) HPLC system (Shimadzu corporation, Japan) and 4500 Q-TRAP mass spectrometer (AB SCIEX, USA). In order to facilitate the subsequent quantification of analytes, a CAP-CELL PAK C_{18} (150 mm × 4.6 mm, 3 μm) connected with a guard column (XB-C_{18}, 10 mm × 4.6 mm, 3 μm), 0.5% formic acid-water (mobile phase A) and acetonitrile (mobile phase B) constituted the chromatographic separation system, and a gradient elution procedure was employed. The elution sequence was as below, 0−10 min, 2-2% B; 10−12 min, 2−12% B; 12−20 min, 12−30% B; 20−25 min, 30−42% B; 25−27 min, 42−65% B; 27−35 min, 65−75% B; 35−38 min, 75−95% B;

38−40 min, 95-2% B; 40−42 min, 2-2% B. 5 μL plasma sample was loaded into the above LC-MS system within a column temperature of 30 °C and a mobile phase flow rate of 0.4 mL/min.

The analytes were fragmentized by an electrospray ion source with a voltage of 5500 eV in the mass spectrometry. After optimizing several mass spectral parameters of each compound, namely, declustering potential (DP), collision energy (CE), and cell exit potential (CXP), all analytes were monitored by negative ion multiple reactions monitoring systems. The optimal DP, CE, and CXP of each ingredient were listed in Table 1.

2.6.2. Plasma samples disposition

Owing to the noteworthy higher content of NAG and HSYA in GHI, we adopted two methods to dispose of plasma samples. One approach was for the quantification of all analytes apart from NAG and HSYA, namely CGA, HYP, K-3-G, K-3-R, pCA, and RT. After 1 μL icariin (5 μg/mL) and 300 μL methanol were added to 100 μL plasma, the mixture was vortexed, and centrifuged at 12000 rpm for 12 min at 4 °C to remove protein. All supernatant was distributed to a new centrifuge tube for subsequent nitrogen blowing. After plasma sample was evaporated dry with nitrogen, 25 μL methanol−water solution (50:50, v/v) was affiliated for re-dissolution. The other approach is for the quantification of NAG and HSYA. The plasma samples in the five anterior time points (i.e., 2, 5, 10, 20, and 40 min) ought to be diluted 200 times to

Table 1. Mass spectrometry conditions of eight analytes and two ISs.

Analytes	Ion mode	Q1 (m/z)	Q3 (m/z)	DP (V)	CE (V)	CXP (V)
Chlorogenic acid	[M−H]⁻	353.0	[a]191.0	−80	−25	−1
			ˆ135.0	−80	−29	−10
Hydroxysafflor yellow A	[M−H]⁻	611.0	[a]491.0	−100	−44	−1
			ˆ403.1	−100	−46	−17
Hyperoside	[M−H]⁻	462.9	[a]299.9	−75	−32	−31
			ˆ271.2	−75	−64	−5
Kaempferol-3-O-glucoside	[M−H]⁻	446.9	[a]283.8	−90	−36	−11
			ˆ227.0	−90	−70	−7
Kaempferol-3-O-rutinoside	[M−H]⁻	593.0	[a]284.8	−80	−38	−19
			ˆ254.9	−80	−62	−9
N-acetyl-L-glutamine	[M−H]⁻	186.9	[a]144.9	−75	−18	−9
			ˆ127.1	−75	−14	−7
p-Coumaric acid	[M−H]⁻	163.1	[a]93.0	−80	−36	−12
			ˆ116.7	−80	−42	−9
Rutin	[M−H]⁻	609.2	[a]300.0	−150	−51	−17
			ˆ271.0	−150	−64	−21
Icariin (IS)	[M-H-Glc]⁻	513.1	[a]366.1	−120	−36	−25
			ˆ323.0	−120	−52	−21
N-carbamoyl-L-glutamate (IS)	[M−H]⁻	188.9	[a]146.1	−80	−16	−9
			ˆ101.7	−80	−26	−7

[a] The ion pairs adopted for quantification, ˆ the ion pairs employed for qualitation.

quantify NAG and HSYA. After 10 μL plasma was diluted 200 times by blank plasma, 1 μL icariin (5 μg/mL), 1 μL NCG (2.5 μg/mL), and 300 μL methanol were entered into 100 μL diluted plasma. The mixture was vortexed, and centrifuged at 12000 rpm for 12 min at 4 °C to remove protein. All supernatant was distributed to a new centrifuge tube to facilitate subsequent nitrogen blowing. And then, 100 μL methanol−water solution (50:50, v/v) was employed to re-dissolve sediment that was blew dry by nitrogen. But the plasma samples in the five latter time points (i.e., 60, 90, 120, 240, and 360 min) only need to be diluted 50 times to quantify NAG and HSYA. Except this, the disposition of plasma samples in the five latter time points for the quantification of NAG and HSYA was the same as the aforementioned.

2.6.3. Internal standard samples, calibration samples, quality control samples, and diluted samples preparation

All standards of analytes and ISs were first dissolved in a methanol-aqueous (50:50, v/v) solution. The concentration of icariin that was applied as IS of CGA, HSYA, HYP, K-3-G, K-3-R, pCA, and RT was 5 μg/mL. The concentration of NCG that was adopted as IS of NAG was 2.5 μg/mL.

The calibration samples were formulated by spiking standard solution with diverse concentrations of eight analytes, as well as standard solution of icariin and NCG into the blank plasma. The final concentrations of CGA, HYP, K-3-G, and RT were all 0.1, 0.5, 1, 5, 10, 50, 100, 500, and 1000 ng/mL, K-3-R, and pCA were both 0.1, 0.5, 1, 5, 10, 50, 100, 500, 1000, 5000, and 10000 ng/mL, while, HSYA and NAG were both 1, 5, 10, 50, 100, 500, 1000, 5000, and 10000 ng/mL, respectively. All calibration samples were adopted for the determination of the linear regression equation of ingredients.

The eight analytes, icariin, and NCG were added into the blank plasma to prepare quality control (QC) samples with three final concentrations of 5, 50, and 500 ng/mL (analytes), 200 ng/mL (icariin), and 100 ng/mL (NCG), respectively. All of the QC samples were adopted for the method validation. The diluted samples were respectively prepared with the final concentration of 500 μg/mL and 2 mg/mL of both NAG and HSYA.

2.6.4. Method validation

In this paper, according to Bioanalytical Method Validation Guidance for Industry (U. S., 2018), we adopted calibration samples, QC samples, and diluted samples to validate LC-MS/MS analytical approach from the following aspects, namely, linear regression, specificity, precision and accuracy, stability, matrix effect, and dilution integrity.

Three samples, namely, blank plasma, drug-contained plasma added with ISs, and blank plasma spiked with mixed standard solution of analytes and ISs, were employed to explore the specificity of analytes and ISs. The calibration samples with a series of concentrations of analytes were adopted to investigate the linear regression equation. Six independent samples of three concentrations of QC samples, i.e., 5, 50, and 500 ng/mL were employed to explore the intra-precision inter-precision, intra-accuracy, and inter-accuracy. For the dilution integrity research, ranges of the upper limit of quantitation of NAG and HSYA were both expanded to 500 μg/mL and 2 mg/mL in consideration of 50-fold and 200-fold dilution, to investigate the precision and accuracy of diluted analytes. QC samples were employed to analyze the stability under multiple store conditions, namely, freeze-thaw stability with three cycles, auto-sampler stability for 24 h at 4 °C, and long-term stability for 1 month at −80 °C. The matrix effect of analytes was ascertained by contrasting the peak area of QC samples and standard solutions with corresponding concentrations.

2.7. Pharmacodynamic research

We employed four myocardial enzymes, CK-MB, IMA, cTn I, and α-HBDH, as the PD indicators to embody the curative effect of GHI on MI/R injury. The level of these biomarkers in plasma was detected by using ELISA kits in the light of manufacturer's instructions.

2.8. Establishment of PLSR model

We encoded NAG, CGA, HSYA, pCA, RT, HYP, K-3-R, and K-3-G as X_1, X_2, X_3, X_4, X_5, X_6, X_7, and X_8, respectively. ΔCK-MB, ΔIMA, ΔcTn I, and Δα-HBDH were considered as different Y to construct partial least squares regression (PLSR) analysis with the help of The Unscrambler X software (version 11) to explore the more profound relationship between analytes with PD indicators [24].

2.9. Exploration of pharmacokinetic parameters and PK/PD model

After analytes were quantified by LC-MS/MS approach, as well as pharmacodynamic indicators were detected by ELISA kits, with the help of Drug and Statistics software (version 3.2.6), we first investigated the PK parameters with a two-

compartment model [10]. The model equations of all PK parameters were listed in formulas 1-11. Owing to the directly detected content of four biomarkers unable to reflect the actual efficacy, with the help of DAS software again, we employed ΔCK-MB, ΔIMA, ΔcTn I, and $\Delta\alpha$-HBDH which represented the deviations of the GHI-administered group with the model group to integrate with PK to establish the optimal PK/PD model by comparing parameters of akaike information criterion (AIC), Schwarz bayesian criterion (SBC), as well as goodness of fit (R^2). In addition, we listed the optimal fitted PK/PD models of analytes that only produce therapeutic effects to each pharmacodynamic indicator according to the results of PLSR analysis in this paper, namely the analytes that possessed a negative coefficient in the PLSR equations.

$$t_{1/2\alpha} = 0.693 \,/\, \alpha \qquad\qquad 1$$

$$t_{1/2\beta} = 0.693 \,/\, \beta \qquad\qquad 2$$

$$V_1 = X_1 \,/\, C_1 \qquad\qquad 3$$

$$V_2 = X_2 \,/\, C_2 \qquad\qquad 4$$

$$CL_1 = kV_1 \qquad\qquad 5$$

$$CL_2 = kV_2 \qquad\qquad 6$$

$$AUC_{(0-t)} = \int_0^t \left(Ae^{-\alpha t} + Be^{-\beta t}\right) dt \qquad\qquad 7$$

$$AUC_{(0-\infty)} = \int_0^\infty \left(Ae^{-\alpha t} + Be^{-\beta t}\right) dt \qquad\qquad 8$$

$$k_{10} = (\alpha\beta(A+B))/(A\beta + B\alpha) \qquad\qquad 9$$

$$k_{12} = \alpha + \beta - k_{10} - k_{21} \qquad\qquad 10$$

$$k_{21} = (A\beta + B\alpha)/(A+B) \qquad\qquad 11$$

$$Q = k_{12}V_1 \qquad\qquad 12$$

2.10. Statistical analysis

By adopting GraphPad Prism 8.0.2 (La Jolla, CA, USA), the discrepancy of data in diverse groups from PD experiment was appraised with an approach of one-way analysis of variance, the concentration–time curve and effect-time bar chart

were presented in a form of mean + standard deviation (SD) [25]. $P < 0.05$ represented conspicuously statistical divergences.

3. Results

3.1. Methodology validation

Illustrated in Supplementary Fig. 1, after a pairwise comparison of three chromatograms of the blank plasma, the drug-contained plasma added with ISs, and the mixed standard solution added with ISs, we successfully qualified the eight analytes in the drug-contained plasma and affirmed that endogenous substances in plasma did not interfere with the detection of analytes and ISs. The linear regression equations were displayed in Supplementary Table 1. All the calibration curves exhibited excellent linearity ($R^2 > 0.99$).

As Supplementary Table 2 shown, the relative standard deviation (RSD) for intra-precision and inter-precision as well as the relative error (RE) for intra-accuracy and inter-accuracy of all analytes were lower than 15%, indicating that the established analytical approach possessed desirable precision and accuracy.

Illustrated in Supplementary Table 3, the RSD of the matrix effect for all analytes was less than 15%, demonstrating that the matrix (plasma) had a minor influence on the quantitative method.

As Supplementary Tables 4-6 shown, the RSD and RE of three kinds of stability (i.e., freeze-thaw stability, auto-sampler stability, and long-term stability) of all analytes were all lower than 15%, indicating that our storage conditions had little effect on the quantification.

As illustrated in Supplementary Table 7, the RE and RSD of HSYA and NAG that were both diluted 50-fold and 200-fold to the concentration of the upper limit was within 15%, affirming that the diluted approach was trustworthy.

3.2. Quantification of eight analytes in GHI

The concentration of eight analytes in GHI was successfully and precisely quantified by the above LC-MS/MS approach. The extracted ion chromatograms of eight analytes and two ISs were presented in Fig. 1. The exact content of eight analytes in GHI was calculated according to the above linear regression equations, which was listed as followed, 30.0 mg/mL (NAG), 1 mg/mL (HSYA), 12.9 μg/mL (CGA), 78.3 μg/mL (pCA), 11.7 μg/mL (RT), 3.4 μg/mL (HYP), 65.7 μg/mL (K-3-R), and 8.7 μg/mL (K-3-
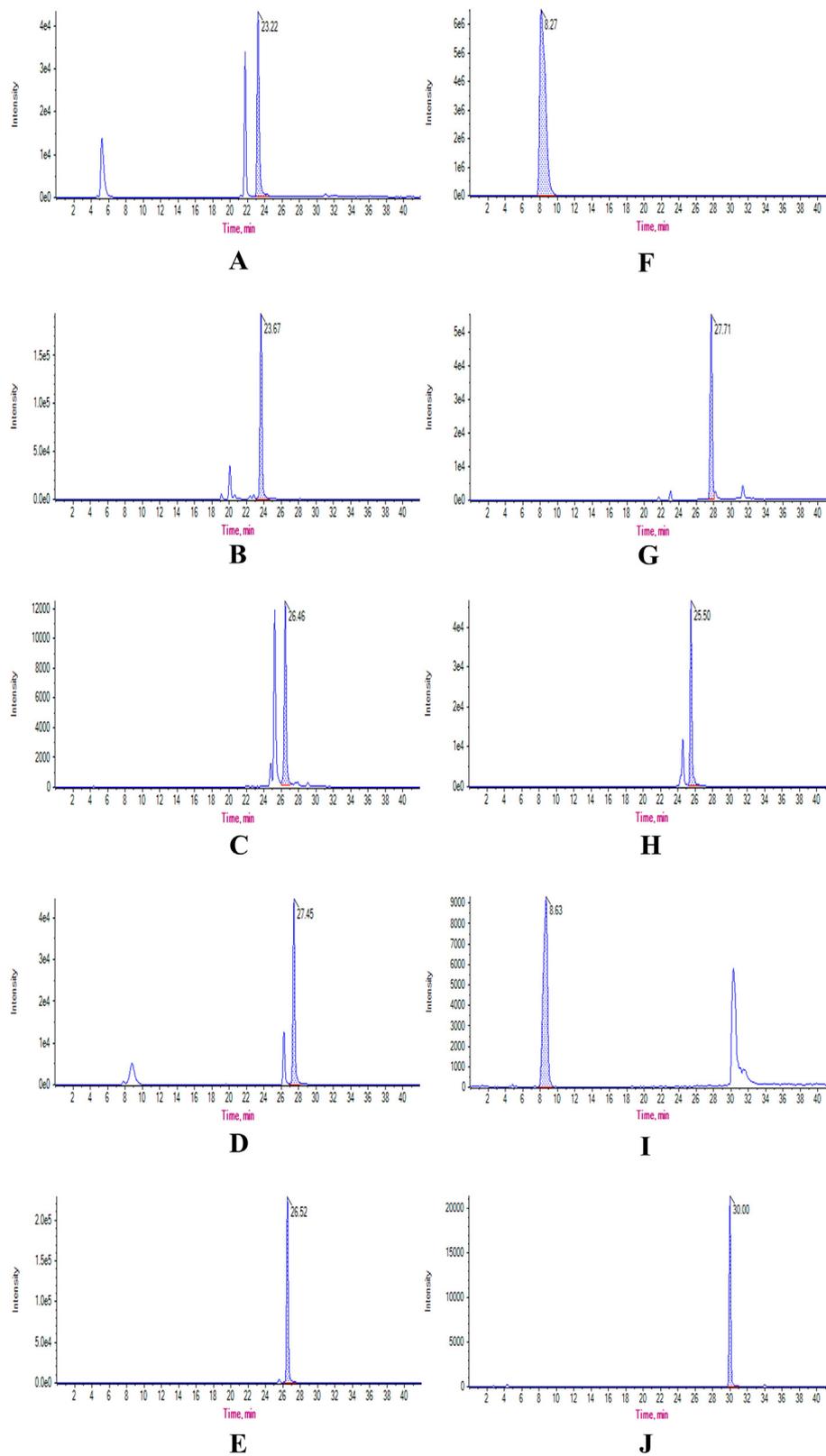
Fig. 1. *Extracted ion chromatograms of eight ingredients and two ISs, including chlorogenic acid (A), hydroxysafflor yellow A (B), hyperoside (C), kaempferol-3-O-glucoside (D), kaempferol-3-O-rutinoside (E), N-acetyl-L-glutamine (F), p-coumaric acid (G), rutin (H), N-carbamoyl-L-glutamate (I), and icariin (J), in GHI detected by LC-MS/MS.*
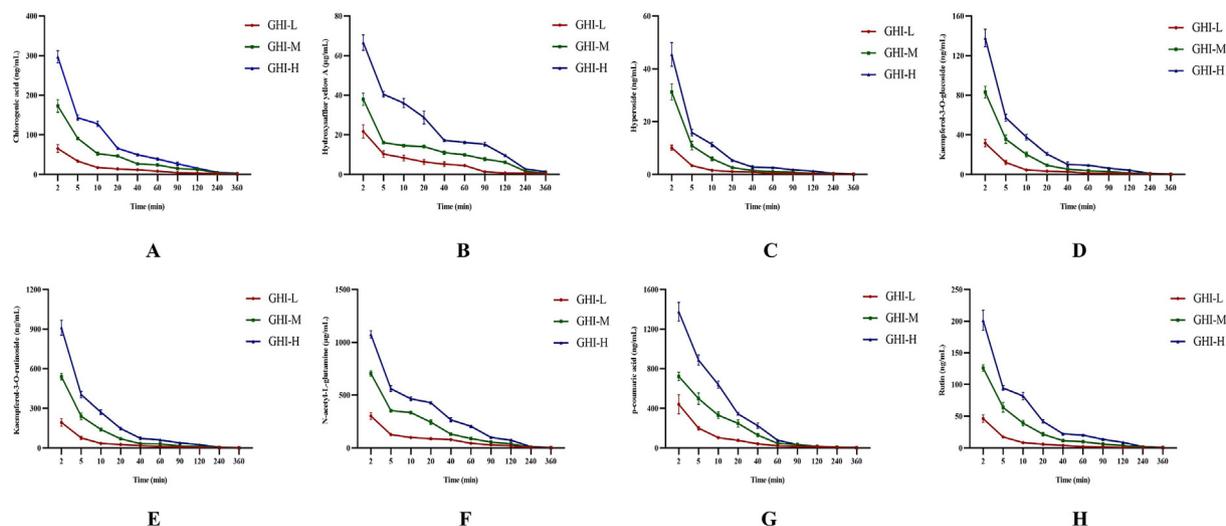
Fig. 2. Plasma concentration–time curves of eight analytes, i.e., chlorogenic acid (A), hydroxysafflor yellow A (B), hyperoside (C), kaempferol-3-O-glucoside (D), kaempferol-3-O-rutinoside (E), N-acetyl-L-glutamine (F), p-coumaric acid (G), rutin (H) (n = 6).

G). The exact concentration of eight analytes that was applied to determine PK parameters was transformed from three different doses of GHI (2.5, 5, and 10 mL/kg) based on the content of eight ingredients in GHI.

3.3. Pharmacokinetic studies

The concentration of eight analytes in plasma was successfully and precisely quantified by the above LC-MS/MS approach. The plasma concentration–time

Table 2. Pharmacokinetic parameters of chlorogenic acid (n = 6).

PK parameters	Chlorogenic acid		
	GHI-L	GHI-M	GHI-H
$t_{1/2\alpha}$ (h)	0.034 ± 0.009	0.031 ± 0.003	0.018 ± 0.003
$t_{1/2\beta}$ (h)	0.919 ± 0.079	0.829 ± 0.121	0.52 ± 0.052
V_1 (L/kg)	0.672 ± 0.201	0.496 ± 0.08	0.389 ± 0.059
V_2 (L/kg)	2.304 ± 0.146	1.49 ± 0.142	1.273 ± 0.103
CL_1 (L/h/kg)	2.669 ± 0.169	1.939 ± 0.146	2.554 ± 0.092
CL_2 (L/h/kg)	8.99 ± 0.907	7.19 ± 0.505	10.403 ± 0.914
$AUC_{(0-t)}$ (µg/L*h)	99.028 ± 52.832	268.98 ± 142.21	408.232 ± 212.364
$AUC_{(0-\infty)}$ (µg/L*h)	102.146 ± 53.386	277.105 ± 142.174	421.197 ± 211.864
K_{10} (1/h)	4.274 ± 1.912	3.987 ± 0.663	6.701 ± 1.078
K_{12} (1/h)	14.327 ± 4.021	14.709 ± 1.766	27.459 ± 6.003
K_{21} (1/h)	3.902 ± 0.294	4.84 ± 0.29	8.203 ± 0.823
Q (L/h/kg)	8.991 ± 0.908	7.190 ± 0.504	10.398 ± 0.912

Table 3. Pharmacokinetic parameters of hydroxysafflor yellow A (n = 6).

PK parameters	Hydroxysafflor yellow A		
	GHI-L	GHI-M	GHI-H
$t_{1/2\alpha}$ (h)	0.017 ± 0.012	0.01 ± 0.003	0.024 ± 0.006
$t_{1/2\beta}$ (h)	0.732 ± 0.1	1.386 ± 0.079	0.972 ± 0.109
V_1 (L/kg)	0.218 ± 0.194	0.126 ± 0.071	0.498 ± 0.088
V_2 (L/kg)	0.838 ± 0.35	1.351 ± 0.099	1.001 ± 0.108
CL_1 (L/h/kg)	1.22 ± 0.369	0.831 ± 0.078	1.13 ± 0.031
CL_2 (L/h/kg)	4.617 ± 2.905	6.72 ± 2.765	9.462 ± 1.509
$AUC_{(0-t)}$ (µg/L*h)	39.625 ± 19.79	112.634 ± 61.077	186.919 ± 99.005
$AUC_{(0-\infty)}$ (µg/L*h)	40.679 ± 19.68	115.716 ± 61.354	190.363 ± 98.813
K_{10} (1/h)	24.474 ± 30.867	9.794 ± 7.36	2.321 ± 0.37
K_{12} (1/h)	41.769 ± 28.827	61.177 ± 16.942	19.794 ± 6.115
K_{21} (1/h)	4.939 ± 2.249	4.88 ± 1.799	9.604 ± 2.209
Q (L/h/kg)	4.621 ± 2.906	6.711 ± 2.762	9.465 ± 1.508

Table 4. Pharmacokinetic parameters of hyperoside (n = 6).

PK parameters	Hyperoside		
	GHI-L	GHI-M	GHI-H
$t_{1/2\alpha}$ (h)	0.023 ± 0.005	0.023 ± 0.005	0.015 ± 0.004
$t_{1/2\beta}$ (h)	0.669 ± 0.077	0.312 ± 0.022	0.313 ± 0.062
V_1 (L/kg)	0.493 ± 0.117	0.34 ± 0.1	0.309 ± 0.126
V_2 (L/kg)	2.979 ± 0.292	0.935 ± 0.119	1.207 ± 0.352
CL_1 (L/h/kg)	5.336 ± 0.493	4.595 ± 0.202	4.915 ± 0.718
CL_2 (L/h/kg)	8.691 ± 0.628	4.573 ± 0.67	7.256 ± 2.273
$AUC_{(0-t)}$ (μg/L*h)	7.719 ± 4.061	17.724 ± 9.103	32.246 ± 15.108
$AUC_{(0-\infty)}$ (μg/L*h)	8.252 ± 4.022	19.295 ± 9.27	34.504 ± 14.937
K_{10} (1/h)	11.259 ± 2.48	14.742 ± 5.174	21.205 ± 16.45
K_{12} (1/h)	18.242 ± 3.358	14.086 ± 2.688	26.235 ± 8.526
K_{21} (1/h)	2.929 ± 0.214	4.889 ± 0.407	6.031 ± 0.862
Q (L/h/kg)	8.690 ± 0.628	4.572 ± 0.672	7.260 ± 2.271

Table 5. Pharmacokinetic parameters of kaempferol-3-O-glucoside (n = 6).

PK parameters	Kaempferol-3-O-glucoside		
	GHI-L	GHI-M	GHI-H
$t_{1/2\alpha}$ (h)	0.026 ± 0.005	0.045 ± 0.024	0.022 ± 0.002
$t_{1/2\beta}$ (h)	0.674 ± 0.094	0.691 ± 0.361	0.385 ± 0.053
V_1 (L/kg)	0.54 ± 0.101	0.59 ± 0.22	0.475 ± 0.044
V_2 (L/kg)	2.822 ± 0.3	1.87 ± 0.735	1.419 ± 0.173
CL_1 (L/h/kg)	5.255 ± 0.593	4.123 ± 0.508	4.4558 ± 0.452
CL_2 (L/h/kg)	7.999 ± 1.661	4.766 ± 1.069	8.474 ± 0.613
$AUC_{(0-t)}$ (μg/L*h)	23.576 ± 12.633	31.49 ± 12.303	116.314 ± 56.651
$AUC_{(0-\infty)}$ (μg/L*h)	25.109 ± 12.653	35.448 ± 11.949	122.652 ± 56.297
K_{10} (1/h)	10.09 ± 2.541	8.042 ± 3.472	9.636 ± 0.934
K_{12} (1/h)	15.148 ± 3.65	9.709 ± 5.342	17.927 ± 1.512
K_{21} (1/h)	2.832 ± 0.492	3.087 ± 1.742	6.02 ± 0.636
Q (L/h/kg)	7.998 ± 1.660	4.764 ± 1.067	8.473 ± 0.613

Table 6. Pharmacokinetic parameters of kaempferol-3-O-rutinoside (n = 6).

PK parameters	Kaempferol-3-O-rutinoside		
	GHI-L	GHI-M	GHI-H
$t_{1/2\alpha}$ (h)	0.024 ± 0.008	0.045 ± 0.025	0.022 ± 0.004
$t_{1/2\beta}$ (h)	0.563 ± 0.116	0.621 ± 0.352	0.348 ± 0.047
V_1 (L/kg)	0.546 ± 0.192	0.603 ± 0.211	0.49 ± 0.094
V_2 (L/kg)	2.437 ± 0.538	1.669 ± 0.725	1.244 ± 0.167
CL_1 (L/h/kg)	5.158 ± 0.266	4.134 ± 0.338	4.481 ± 0.265
CL_2 (L/h/kg)	9.313 ± 2.573	4.919 ± 1.189	8.486 ± 0.614
$AUC_{(0-t)}$ (μg/L*h)	163.614 ± 83.456	211.446 ± 86.297	778.474 ± 381.478
$AUC_{(0-\infty)}$ (μg/L*h)	172.917 ± 84.754	236.738 ± 84.799	819.682 ± 380.899
K_{10} (1/h)	10.77 ± 4.722	7.644 ± 2.745	9.381 ± 1.601
K_{12} (1/h)	19.134 ± 9.171	9.432 ± 4.449	17.849 ± 3.532
K_{21} (1/h)	3.903 ± 1.019	3.686 ± 2.064	6.923 ± 0.999
Q (L/h/kg)	9.311 ± 2.570	4.919 ± 1.190	8.485 ± 0.615

curves of eight analytes in GHI-administered groups were exhibited in Fig. 2. The PK parameters that primarily reflect the characteristics of distribution and elimination of eight analytes were listed in Tables 2−9, including half-life ($t_{1/2}$), apparent volume of distribution (V), clearance (CL), area under the concentration−time curve (AUC), and elimination rate constant (Ke). From the results of PK parameters, it was obvious to discover the values of $t_{1/2\beta}$, k_{12}, V_2, and CL_2 were larger than those of $t_{1/2\alpha}$, k_{21}, V_1, and CL_1 for all compounds in GHI under all three different dosages. For all parameters of the eight ingredients, only $AUC_{(0-t)}$ and $AUC_{(0-\infty)}$ presented obvious dose-dependence, while, the variant trend of the other parameters had its own charms with the transformation of the dosage of GHI.

Table 7. Pharmacokinetic parameters of N-acetyl-L-glutamine (n = 6).

PK parameters	N-acetyl-L-glutamine		
	GHI-L	GHI-M	GHI-H
$t_{1/2\alpha}$ (h)	0.014 ± 0.003	0.005 ± 0.001	0.018 ± 0.011
$t_{1/2\beta}$ (h)	0.814 ± 0.078	0.462 ± 0.023	0.709 ± 0.083
V_1 (L/kg)	0.223 ± 0.057	0.024 ± 0.008	0.339 ± 0.204
V_2 (L/kg)	1.381 ± 0.093	0.445 ± 0.069	1.144 ± 0.167
CL_1 (L/h/kg)	1.577 ± 0.116	1.133 ± 0.122	1.633 ± 0.135
CL_2 (L/h/kg)	8.185 ± 1.181	1.776 ± 0.548	8.632 ± 3.038
$AUC_{(0-t)}$ (µg/L*h)	538.219 ± 290.308	1012.749 ± 472.353	1048.88 ± 551.764
$AUC_{(0-\infty)}$ (µg/L*h)	553.382 ± 290.017	1060.065 ± 473.211	1079.308 ± 551.248
K_{10} (1/h)	7.691 ± 3.042	50.018 ± 3.042	9.543 ± 11.62
K_{12} (1/h)	38.711 ± 10.279	73.95 ± 2.602	37.368 ± 24.261
K_{21} (1/h)	5.932 ± 0.785	3.913 ± 0.6	7.43 ± 2.404
Q (L/h/kg)	8.185 ± 1.181	1.771 ± 0.553	8.631 ± 3.051

Table 8. Pharmacokinetic parameters of p-coumaric acid (n = 6).

PK parameters	p-Coumaric acid		
	GHI-L	GHI-M	GHI-H
$t_{1/2\alpha}$ (h)	0.03 ± 0.009	0.037 ± 0.025	0.034 ± 0.01
$t_{1/2\beta}$ (h)	0.487 ± 0.059	0.392 ± 0.084	0.321 ± 0.049
V_1 (L/kg)	0.462 ± 0.17	0.677 ± 0.122	0.723 ± 0.095
V_2 (L/kg)	1.272 ± 0.124	0.7 ± 0.142	0.669 ± 0.07
CL_1 (L/h/kg)	3.317 ± 0.369	2.808 ± 0.134	3.469 ± 0.187
CL_2 (L/h/kg)	5.909 ± 1.304	6.918 ± 2.46	6.658 ± 2.185
$AUC_{(0-t)}$ (µg/L*h)	380.718 ± 210.96	942.029 ± 503.001	1526.046 ± 777.772
$AUC_{(0-\infty)}$ (µg/L*h)	400.705 ± 216.195	969.468 ± 504.903	1579.385 ± 775.148
K_{10} (1/h)	8.039 ± 2.934	4.277 ± 0.897	4.878 ± 0.808
K_{12} (1/h)	14.117 ± 4.736	11.023 ± 5.384	9.545 ± 4.156
K_{21} (1/h)	4.662 ± 1.024	10.302 ± 3.876	10.071 ± 3.659
Q (L/h/kg)	5.909 ± 1.300	6.919 ± 2.461	6.656 ± 2.183

Table 9. Pharmacokinetic parameters of rutin (n = 6).

PK parameters	Rutin		
	GHI-L	GHI-M	GHI-H
$t_{1/2\alpha}$ (h)	0.024 ± 0.002	0.035 ± 0.01	0.012 ± 0.006
$t_{1/2\beta}$ (h)	0.541 ± 0.055	0.492 ± 0.082	0.348 ± 0.047
V_1 (L/kg)	0.379 ± 0.071	0.466 ± 0.88	0.239 ± 0.209
V_2 (L/kg)	1.671 ± 0.12	1.075 ± 0.133	0.855 ± 0.277
CL_1 (L/h/kg)	3.795 ± 0.496	2.872 ± 0.264	2.813 ± 0.459
CL_2 (L/h/kg)	6.267 ± 0.809	5.018 ± 0.665	6.712 ± 3.688
$AUC_{(0-t)}$ (µg/L*h)	34.647 ± 19.017	124.334 ± 65.117	209.185 ± 106.205
$AUC_{(0-\infty)}$ (µg/L*h)	36.886 ± 19.221	129.725 ± 65.166	217.984 ± 105.554
K_{10} (1/h)	10.125 ± 0.978	6.448 ± 1.858	25.55 ± 19.846
K_{12} (1/h)	16.754 ± 1.998	11.318 ± 3.536	42.24 ± 19.866
K_{21} (1/h)	3.748 ± 0.381	4.751 ± 1.024	7.333 ± 1.971
Q (L/h/kg)	6.267 ± 0.813	5.018 ± 0.665	6.706 ± 3.691

3.4. Pharmacodynamic studies

The myocardial injured markers, CK-MB, IMA, cTn I, and α-HBDH, were quantified according to manufacturer's instructions via adopting ELISA kits. The obtained standard curve equations were as follows: $y = 0.1425x + 0.1193$ ($R^2 = 0.9992$) for CK-MB; $y = 0.0235x + 0.1444$ ($R^2 = 0.9987$) for IMA; $y = 0.3709x + 0.2161$ ($R^2 = 0.9896$) for cTn I; and $y = 0.0358x + 0.166$ ($R^2 = 0.9959$) for α-HBDH. As shown in Fig. 3, the four biomarkers in the model group were dramatically up-regulated compared with the sham group within 2–360 min of blood collection, indicating that MI/R model was triumphantly established. The pharmacodynamic action of GHI on each marker was apparently different,
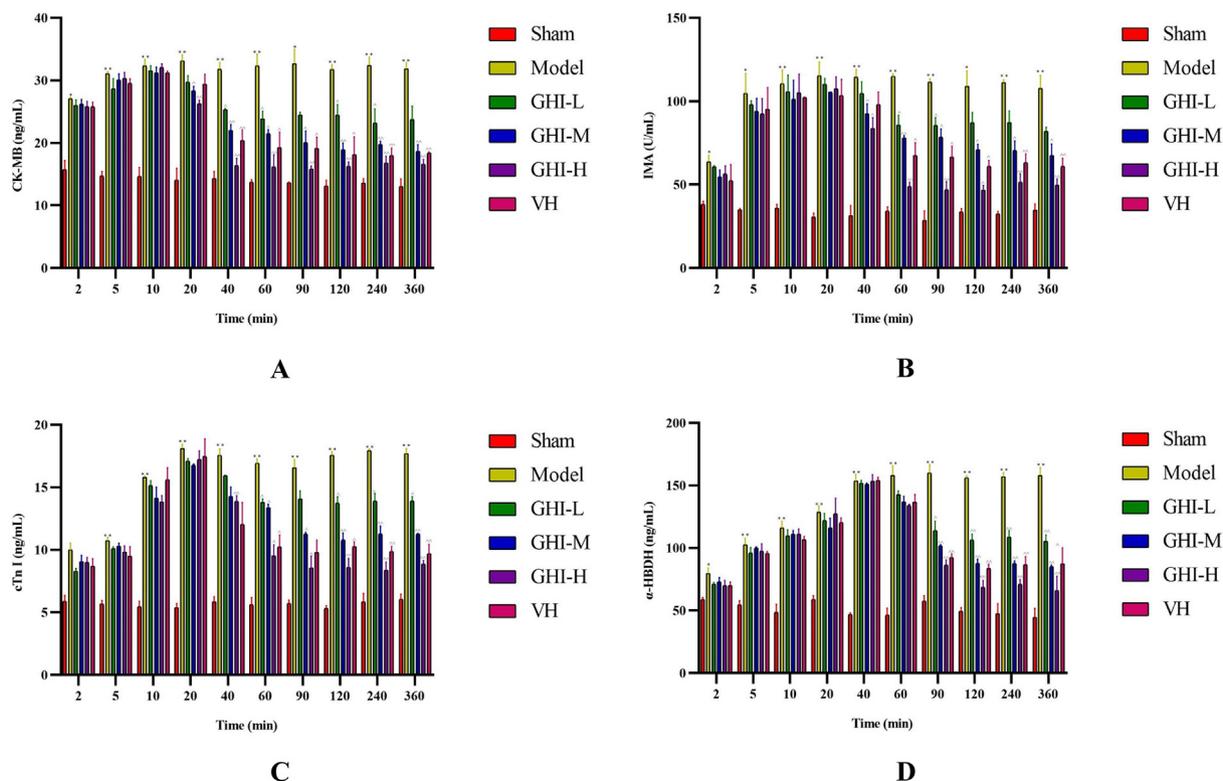
Fig. 3. Quantification for the myocardial injured biomarkers of CK-MB (A), IMA (B), cTn I (C), and α-HBDH (D) (n = 3). **/*P < 0.01/0.05 vs. sham group; ^^/^P < 0.01/0.05 vs. model group.

which was primarily reflected in the time for the first decline in the content of each marker. For CK-MB, the content descended at 20 min after administrating GHI. The content of both IMA and cTn I presented a downward trend at 40 min after GHI administration. The reduction of α-HBDH that began at 60 min after GHI treatment was the latest. We speculated that this difference may be related to the inconsistent tempo on distribution and metabolism of diverse effective compounds in GHI in tissues. Furthermore, the regulation of GHI on the four biomarkers also appeared demonstrable dose-dependence. As far as the four biomarkers, the cardioprotection of high-dose GHI was better than the positive control medication, verapamil hydrochloride.

3.5. Results of PLSR analysis

The PLSR equations of analytes and PD indicators was explored by us with the help of The Unscrambler X software (version 11). All PLSR equations that respectively considered ΔCK-MB, ΔIMA, ΔcTn I, and Δα-HBDH as Y were listed in Table 10. The predicted results of PLSR for each compound and each myocardial enzymes were listed in Figs. 5—7.

The weighted regression coefficients that reacted the correlation of analytes and PD indicators were illustrated in Figs. 8—10. The plus-minus of co-efficients represented the positive and negative relation between analytes and PD indicators. Due to the curative effect of GHI embodied in the reduction of CK-MB, IMA, cTn I, and α-HBDH in the present research, we focused on analytes with minus co-efficients. After statistics and analysis of weighted regression coefficients, we discovered NAG, HSYA, CGA, and pCA were mostly positively correlated with the decline of the four biomarkers, so these four ingredients played a more indispensable role when GHI treating MI/R injury.

3.6. Establishment of PK/PD models

We regarded the concentration of each analyte as X-axis, and the concentration of each PD indicator as Y-axis to sketch the curve. As Fig. 4 shown, the cardioprotection of GHI was invariably exerted later approximately 2—4 time points (i.e., from 10 min to 40 min) than the first blood collection point. This phenomenon was caused by the unique character-istics of distribution of each analyte. We adopted the Sigmoid-E_{max} model to integrate PK and PD, and

Table 10. PLSR equations for all analytes respectively with ΔCK-MB, ΔIMA, ΔcTn I, and Δα-HBDH.

Dependent variables	Groups	PLSR equations
ΔCK-MB	GHI-L	$Y = -1.36649X_1 + 2.420342X_2 - 0.1390197X_3 - 3.597929X_4 + 0.4765264X_5 + 2.2475471X_6 - 1.347652X_7 + 0.6581857X_8$
	GHI-M	$Y = -0.7705629X_1 - 0.0237398X_2 - 0.1541825X_3 - 1.022269X_4 - 0.0849163X_5 + 0.6763485X_6 + 0.2053435X_7 + 0.3452763X_8$
	GHI-H	$Y = 0.2855634X_1 - 0.1449057X_2 - 0.2111469X_3 - 1.850764X_4 - 0.3616633X_5 + 0.9251882X_6 + 0.0224434X_7 + 0.5270877X_8$
ΔIMA	GHI-L	$Y = -0.6954968X_1 - 0.3810411X_2 - 0.9159328X_3 - 0.2133788X_4 + 0.3320674X_5 + 0.7109738X_6 + 0.089624X_7 + 0.4898437X_8$
	GHI-M	$Y = -0.7402096X_1 + 0.0381992X_2 - 0.4412489X_3 - 1.018898X_4 + 0.0597021X_5 + 0.6760102X_6 + 0.3246165X_7 + 0.4088811X_8$
	GHI-H	$Y = -1.176141X_1 - 0.3651575X_2 + 0.4547408X_3 - 1.68081X_4 + 0.2217712X_5 + 0.9449685X_6 + 0.2036869X_7 + 0.679628X_8$
ΔcTn I	GHI-L	$Y = -2.603504X_1 + 1.548511X_2 - 0.2964474X_3 - 2.511441X_4 - 0.2679573X_5 + 3.7428298X_6 + 0.6550613X_7 - 0.7299335X_8$
	GHI-M	$Y = -0.7136006X_1 - 0.1127803X_2 - 0.5595503X_3 - 0.9280757X_4 + 0.0124179X_5 + 0.7685454X_6 + 0.321465X_7 + 0.44222X_8$
	GHI-H	$Y = -1.660466X_1 + 0.0560317X_2 + 0.1925077X_3 - 1.501105X_4 + 0.4283781X_5 + 0.9009857X_6 + 0.1821965X_7 + 0.6318244X_8$
Δα-HBDH	GHI-L	$Y = -0.9408289X_1 - 0.879114X_2 - 1.268848X_3 - 0.1344323X_4 + 0.578991X_5 + 1.0949033X_6 + 0.1299974X_7 + 0.8911269X_8$
	GHI-M	$Y = -0.7603841X_1 - 0.0563754X_2 - 0.8696728X_3 - 0.8624248X_4 + 0.1017748X_5 + 0.8386844X_6 + 0.422355X_7 + 0.5269656X_8$
	GHI-H	$Y = -2.673813X_1 - 0.8999723X_2 + 0.5539879X_3 - 0.6081021X_4 + 0.3924785X_5 + 1.0899045X_6 + 0.4757133X_7 + 1.0647134X_8$

PK/PD equations were expressed in the form of "$E = E_{max} * C^\gamma/(ED_{50}^\gamma + C^\gamma)$", in which E_{max} represented the maximal effect of the drug, ED_{50} meant the drug concentration when achieving the half effect of E_{max}, and γ symbolized the slope of PK/PD curve. By comparing the parameters, AIC, SBC, and R^2, generated from altering the compartmental model and weight coefficient, the optimal


A	B	C
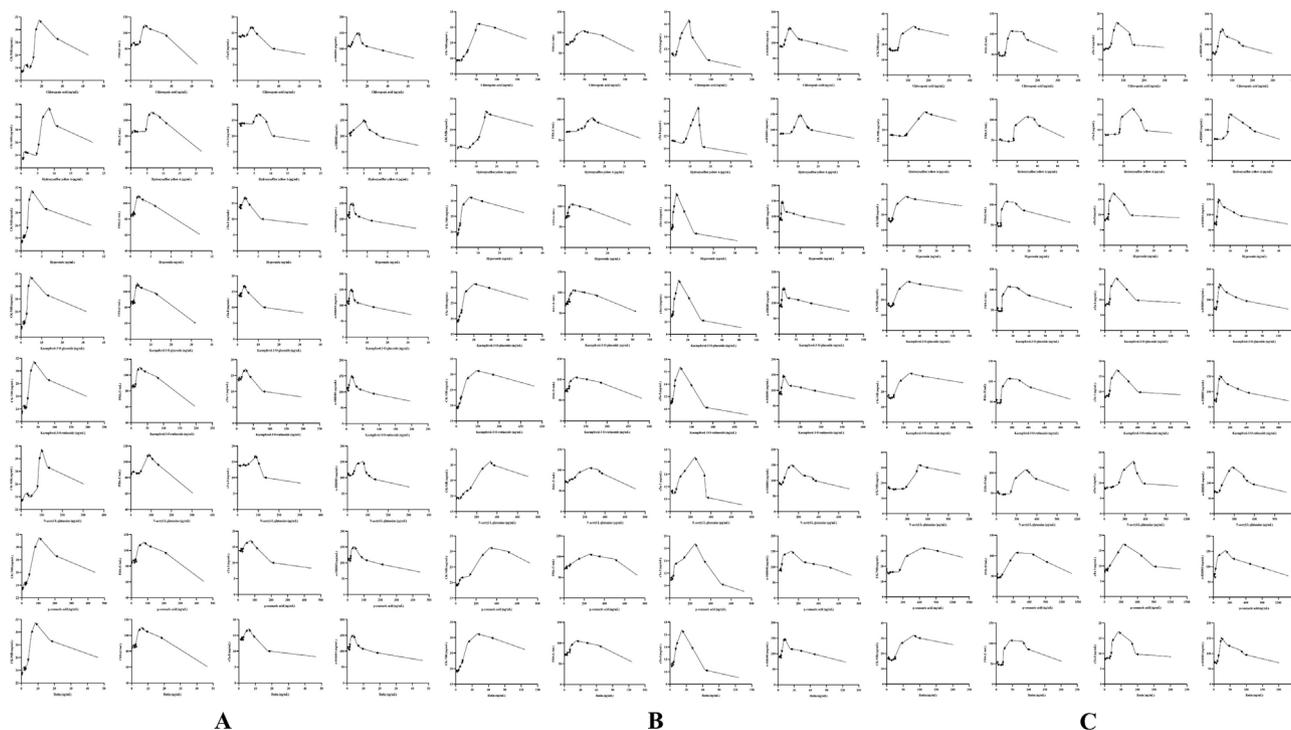
Fig. 4. Diagram of PK/PD correlation in GHI-L group (A), GHI-M group (B), and GHI-H group (C).
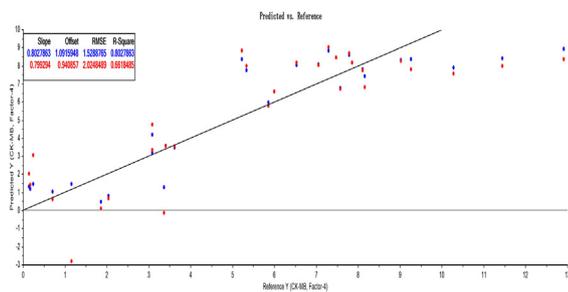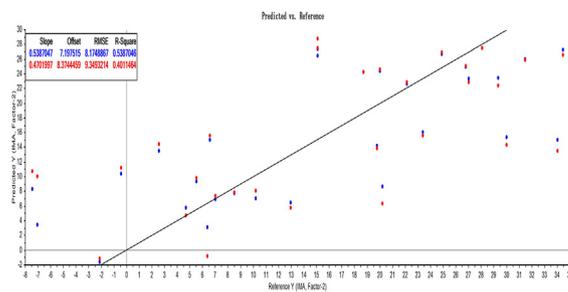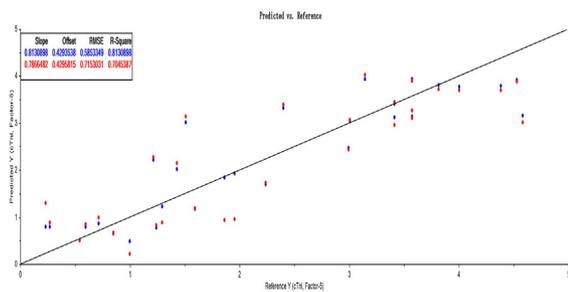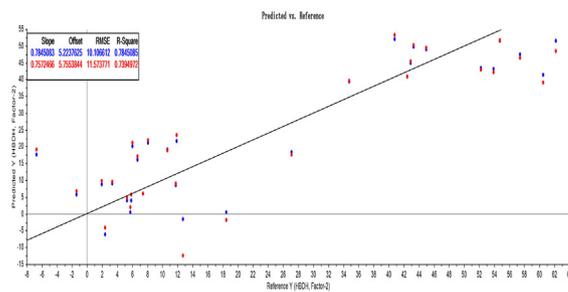
Fig. 5. Predicted results of PLSR for analytes and ΔCK-MB (A), ΔIMA (B), ΔcTn I (C), and Δα-HBDH (D) in GHI-L group.
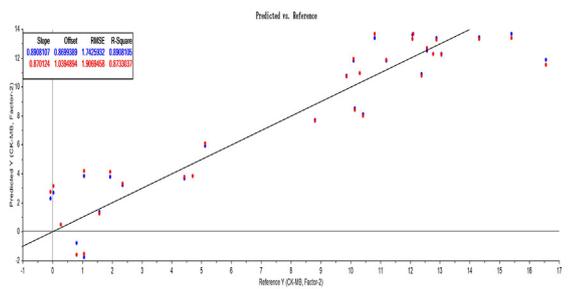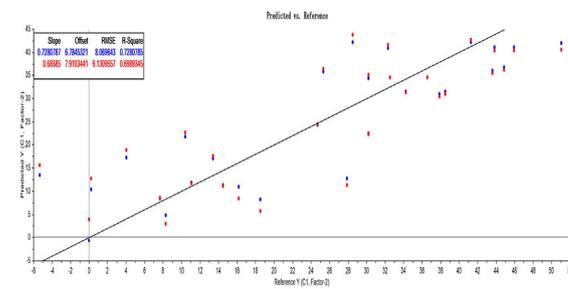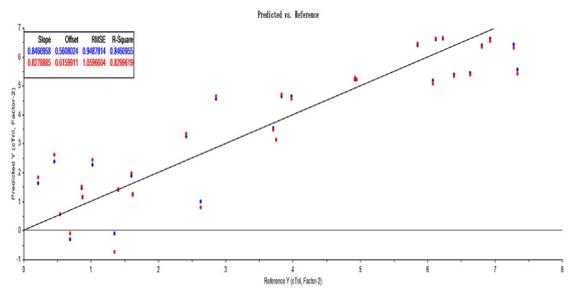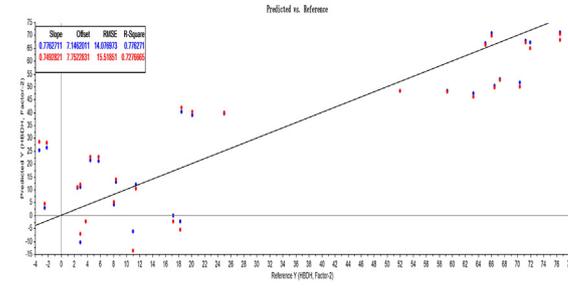
Fig. 6. Predicted results of PLSR for analytes and ΔCK-MB (A), ΔIMA (B), ΔcTn I (C), and Δα-HBDH (D) in GHI-M group.

A

B

C

D
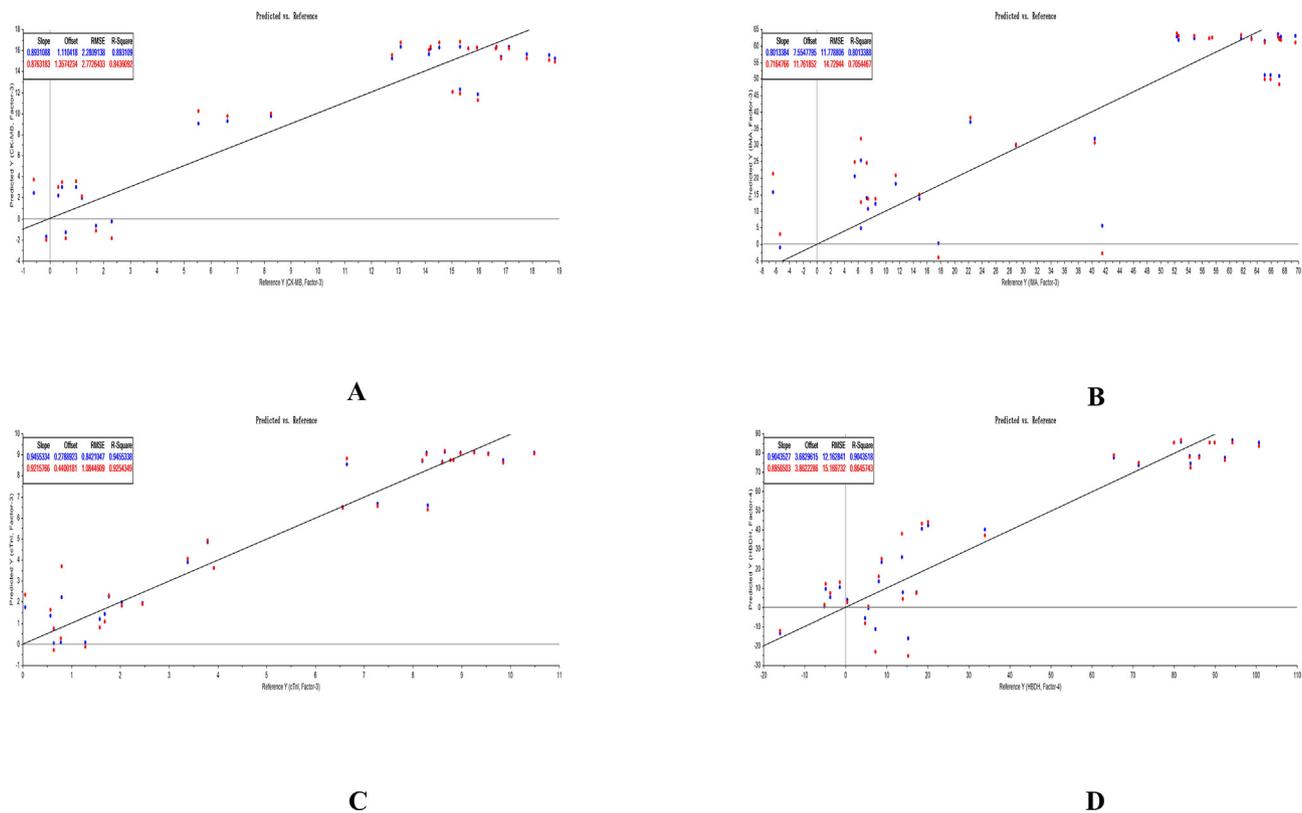
Fig. 7. Predicted results of PLSR for analytes and ΔCK-MB (A), ΔIMA (B), ΔcTn I (C), and Δα-HBDH (D) in GHI-H group.

A

B

C

D
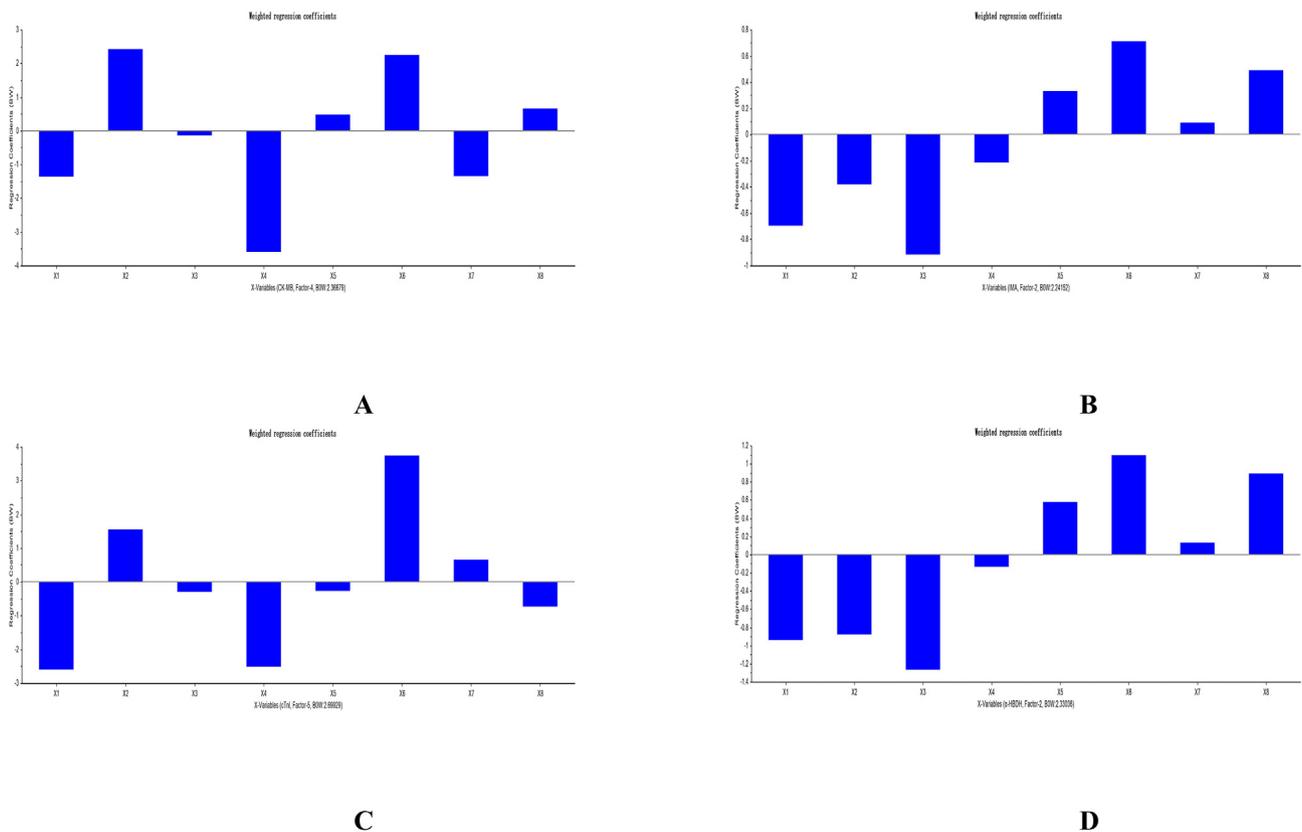
Fig. 8. Weighted regression coefficients of analytes and ΔCK-MB (A), ΔIMA (B), ΔcTn I (C), and Δα-HBDH (D) in GHI-L group.
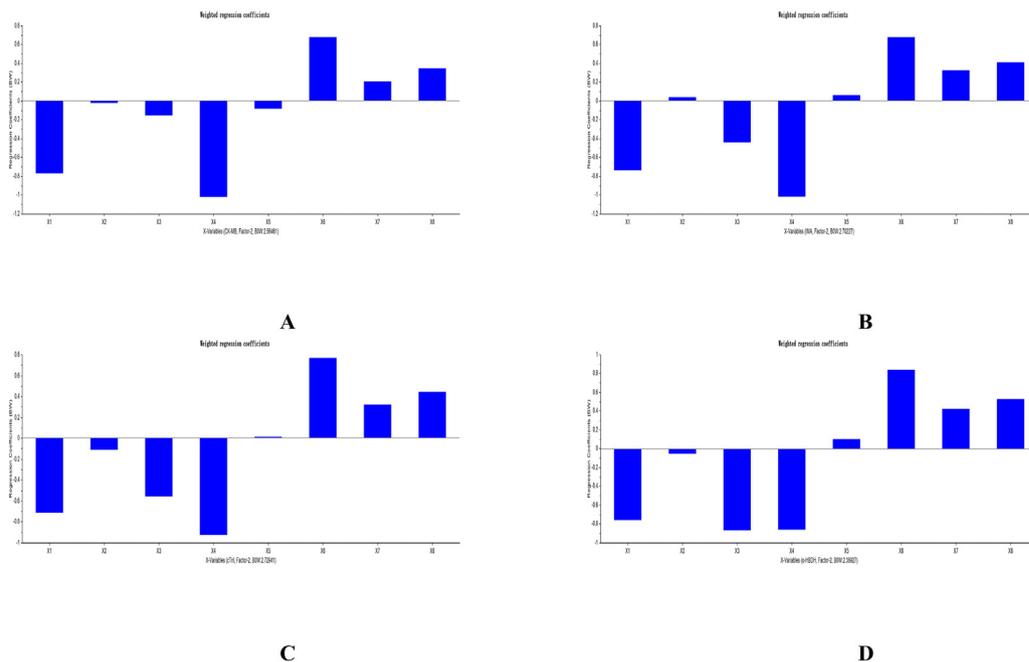
Fig. 9. Weighted regression coefficients of analytes and Δ CK-MB (A), Δ IMA (B), Δ cTn I (C), and Δ α-HBDH (D) in GHI-M group.
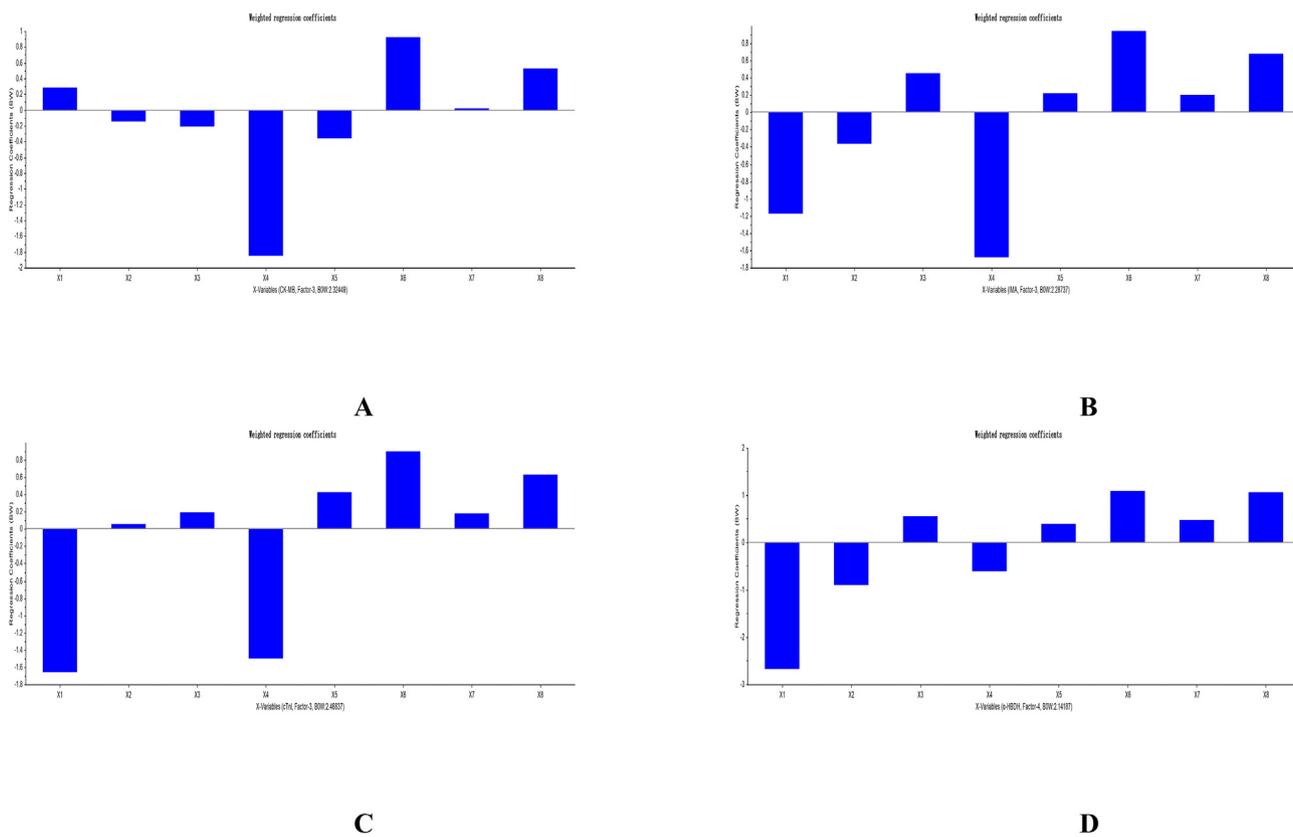
Fig. 10. Weighted regression coefficients of analytes and Δ CK-MB (A), Δ IMA (B), Δ cTn I (C), and Δ α-HBDH (D) in GHI-H group.

Table 11. *The value of parameters of AIC, SBC, and R^2 of the optimal PK/PD model for all analytes with ΔCK-MB, ΔIMA, ΔcTn I, and $\Delta\alpha$-HBDH.*

Analytes	Groups	AIC	SBC	R^2
	GHI-L	−4.959	−3.144	0.999
Chlorogenic acid	GHI-M	14.18	15.996	0.998
	GHI-H	28.481	30.297	0.995
	GHI-L	12.894	14.71	0.993
Hydroxysafflor yellow A	GHI-M	−4.715	−2.9	0.999
	GHI-H	41.97	43.786	0.994
	GHI-L	−13.047	−11.232	0.999
Hyperoside	GHI-M	9.67	11.486	0.999
	GHI-H	−0.551	1.264	0.999
	GHI-L	−13.161	−11.346	0.999
Kaempferol-3-O-glucoside	GHI-M	−8.287	−6.472	0.999
	GHI-H	10.973	12.788	0.999
	GHI-L	7.092	8.908	0.999
Kaempferol-3-O-rutinoside	GHI-M	−8.252	−6.436	0.999
	GHI-H	27.25	29.065	0.999
	GHI-L	25.188	27.003	0.997
N-acetyl-L-glutamine	GHI-M	83.141	84.956	0.997
	GHI-H	34.885	36.701	0.998
	GHI-L	−13.529	−11.713	0.999
p-Coumaric acid	GHI-M	35.145	36.961	0.998
	GHI-H	96.997	98.812	0.998
	GHI-L	18.369	20.185	1.000
Rutin	GHI-M	−12.21	−10.395	0.999
	GHI-H	21.725	23.541	0.995

PK/PD equation was determined. We discovered that values of the above parameters of the optimal PK/PD models generated by fitting eight ingredients with each PD indicator were the same, which were listed in Table 11. The optimum PK/PD equations of analytes with a negative coefficient in PLSR equations that were integrated with ΔCK-MB, ΔIMA, ΔcTn I, and $\Delta\alpha$-HBDH were respectively listed in Tables 12–15. After comparing the variation of parameters in PK/PD equations when the dose of GHI was gradually magnified, we discovered that E_{max}

and ED_{50} of most ingredients raised when the dose of GHI was magnified. There was no significant trend of γ when the dose of GHI was continuously elevated.

4. Discussion

In this study, we established a well-performance LC-MS/MS approach to quantify eight ingredients in plasma after administrating three kinds of doses of GHI and contrasted their PK parameters. AUC, one momentous PK parameter, reflects the amount of drug that enters the systemic circulation to represent the exploited degree of medication [26]. The ascension of $AUC_{(0-t)}$ and $AUC_{(0-\infty)}$ of eight analytes indicated that the exploited drug concentration in tissues was gradually enlarged with the increment of the dose of GHI. $T_{1/2\alpha}$ and $t_{1/2\beta}$, both belong to half-life, but respectively reflect the speed of distribution and elimination of drugs in the organism [27]. The value of $t_{1/2\beta}$ was larger than $t_{1/2\alpha}$ for all ingredients, indicating all analyzed components in GHI possessed a feature of rapid distribution and slow elimination.

Two constants, k_{12} and k_{21}, reflect the rate of transfer of drugs, in which k_{12} represents the rate of drugs transported from the central compartment to the peripheral compartment, and k_{21} symbolizes the rate of drugs transferred from the peripheral compartment to the central compartment [28]. After comparing the values of k_{12} and k_{21} of all ingredients, we intriguingly found that the value of k_{12} of each compound was larger than that of k_{21}, and all analytes were divided into two kinds according to their variant tendency of k_{12} and k_{21} with the enhancement of the dose of GHI. One kind was to promote ingredients to centralize in the central compartment owing to the decrease of k_{12} and the increase of k_{21}, including NAG, HSYA, K-3-R, and

Table 12. *Equations of the optimal PK/PD model between analytes with negative coefficient in PLSR equations and ΔCK-MB.*

Groups	Analytes	Optimal equations
GHI-L	N-acetyl-L-glutamine	$E = 11.04 * C^{0.077}/(23.588^{0.077} + C^{0.077})$
	Hydroxysafflor yellow A	$E = 11.082 * C^{0.071}/(1.708^{0.071} + C^{0.071})$
	p-Coumaric acid	$E = 6.058 * C^{0.098}/(36.418^{0.098} + C^{0.098})$
	Kaempferol-3-O-rutinoside	$E = 11.04 * C^{0.081}/(14.175^{0.081} + C^{0.081})$
GHI-M	N-acetyl-L-glutamine	$E = 13.089 * C^{0.096}/(87.945^{0.096} + C^{0.096})$
	Chlorogenic acid	$E = 11.972 * C^{1.907}/(14.044^{1.907} + C^{1.907})$
	Hydroxysafflor yellow A	$E = 27.2 * C^{0.31}/(8.993^{0.31} + C^{0.31})$
	p-Coumaric acid	$E = 15.943 * C^{0.238}/(135.185^{0.238} + C^{0.238})$
	Rutin	$E = 11.991 * C^{1.357}/(4.448^{1.357} + C^{1.357})$
GHI-H	Chlorogenic acid	$E = 16.037 * C^{1.302}/(32.041^{1.302} + C^{1.302})$
	Hydroxysafflor yellow A	$E = 15.892 * C^{1.189}/(14.57^{1.189} + C^{1.189})$
	p-Coumaric acid	$E = 15.798 * C^{0.034}/(681.918^{0.034} + C^{0.034})$
	Rutin	$E = 15.908 * C^{1.459}/(17.239^{1.459} + C^{1.459})$

Table 13. *Equations of the optimal PK/PD model between analytes with negative coefficient in PLSR equations and ΔIMA.*

Groups	Analytes	Optimal equations
GHI-L	N-acetyl-L-glutamine	$E = 31.136 * C^{0.055}/(34.028^{0.055} + C^{0.055})$
	Chlorogenic acid	$E = 28.211 * C^{0.102}/(0.01^{0.102} + C^{0.102})$
	Hydroxysafflor yellow A	$E = 31.473 * C^{0.036}\gamma/(31.952^{0.036} + C^{0.036})$
	p-Coumaric acid	$E = 19.558 * C^{0.025}/(57.234^{0.025} + C^{0.025})$
GHI-M	N-acetyl-L-glutamine	$E = 42.733 * C^{0.01}/(257.817^{0.01} + C^{0.01})$
	Hydroxysafflor yellow A	$E = 49.851 * C^{0.26}/(0.284^{0.26} + C^{0.26})$
	p-Coumaric acid	$E = 49.851 * C^{0.117}/(152.996^{0.117} + C^{0.117})$
GHI-H	N-acetyl-L-glutamine	$E = 77.916 * C^{0.398}/(278.429^{0.398} + C^{0.398})$
	Chlorogenic acid	$E = 65.739 * C^{2.091}/(26.917^{2.091} + C^{2.091})$
	p-Coumaric acid	$E = 62.712 * C^{0.031}/(579.064^{0.031} + C^{0.031})$

Table 14. *Equations of the optimal PK/PD model between analytes with negative coefficient in PLSR equations and ΔcTn I.*

Groups	Analytes	Optimal equations
GHI-L	N-acetyl-L-glutamine	$E = 4.608 * C^{0.037}/(39.987^{0.037} + C^{0.037})$
	Hydroxysafflor yellow A	$E = 4.628 * C^{0.021}/(2.576^{0.021} + C^{0.021})$
	p-Coumaric acid	$E = 2.907 * C^{0.01}/(37.91^{0.01} + C^{0.01})$
	Rutin	$E = 4.632 * C^{0.01}/(2.595^{0.01} + C^{0.01})$
	Kaempferol-3-O-glucoside	$E = 4.625 * C^{0.01}/(1.17^{0.01} + C^{0.01})$
GHI-M	N-acetyl-L-glutamine	$E = 6.714 * C^{0.035}/(79.994^{0.035} + C^{0.035})$
	Chlorogenic acid	$E = 7.28 * C^{0.039}/(14.36^{0.039} + C^{0.039})$
	Hydroxysafflor yellow A	$E = 7.341 * C^{0.13}/(2.191^{0.13} + C^{0.13})$
	p-Coumaric acid	$E = 7.258 * C^{0.052}/(107.805^{0.052} + C^{0.052})$
GHI-H	N-acetyl-L-glutamine	$E = 10.158 * C^{0.228}/(273.62^{0.228} + C^{0.228})$
	p-Coumaric acid	$E = 9.007 * C^{0.146}/(161.46^{0.146} + C^{0.146})$

Table 15. *Equations of the optimal PK/PD model between analytes with negative coefficient in PLSR equations and Δα-HBDH.*

Groups	Analytes	Optimal equations
GHI-L	N-acetyl-L-glutamine	$E = 48.85 * C^{0.023}/(39.96^{0.023} + C^{0.023})$
	Chlorogenic acid	$E = 48.745 * C^{0.079}/(0.01^{0.079} + C^{0.079})$
	Hydroxysafflor yellow A	$E = 49.45 * C^{0.049}/(0.01^{0.049} + C^{0.049})$
	p-Coumaric acid	$E = 37.993 * C^{0.01}/(48.824^{0.01} + C^{0.01})$
GHI-M	N-acetyl-L-glutamine	$E = 72.312 * C^{0.01}/(211.779^{0.01} + C^{0.01})$
	Chlorogenic acid	$E = 72.774 * C^{0.099}/(6.693^{0.099} + C^{0.099})$
	Hydroxysafflor yellow A	$E = 88.223 * C^{0.236}/(0.608^{0.236} + C^{0.236})$
	p-Coumaric acid	$E = 71.86 * C^{0.075}/(95.976^{0.075} + C^{0.075})$
GHI-H	N-acetyl-L-glutamine	$E = 91.925 * C^{0.136}/(154.598^{0.136} + C^{0.136})$
	Chlorogenic acid	$E = 86.524 * C^{0.194}/(26.016^{0.194} + C^{0.194})$
	p-Coumaric acid	$E = 89.907 * C^{0.01}/(663.126^{0.01} + C^{0.01})$

pCA. The other kind was to facilitate components to permeate into the peripheral compartment due to the increase of k_{12} and the decrease of k_{21}, containing CGA, HYP, K-3-G, and RT. We deemed this phenomenon may be led by the content difference among all analytes in GHI. Each ingredient bore the brunt of distribution in the peripheral compartment after administrating GHI. The components with a low content were principally dispersed in the peripheral compartment, while the compounds with a high content funneled into the central compartment after fulfilling the peripheral compartment.

Another PK parameter, V, evaluated the distribution range of drugs according to the numeric value. The lower V value manifested drugs were predominantly distributed in blood, while the higher V value indicated drugs were extensively assimilated by tissues [29]. In our current research, the value of V_2 of all components was larger than V_1, proclaiming that all analytes primarily existed in tissues in the peripheral compartment. What's more fascinating was that only the values of V_1 and V_2 of HSYA enlarged among all analytes with the upbeat of the dose of GHI, suggesting that the ingested ability of tissues for it was optimal among all compounds. Due to the same tendency of V_2 of all ingredients except for the extraordinary HSYA, we separated the other analytes into four groups in the light of their variable tend of V_1 with the promotion of the dose of GHI. The first kind was ingredients

converged in the blood of the central compartment embodied in the mere decline of V_1, including CGA and HYP. The second kind was compounds scattered in tissues of the central compartment reflected by the pure rise of V_1, such as pCA. The third kind and the last kind were components (i.e., K-3-G, K-3-R, and RT) with first increased and then decreased V_1 and constituents (i.e., NAG) with first decreased and then increased V_1, respectively. We believed this outcome was induced by the speed of ingestion of NAG by tissues was faster than other compositions. Hence, we weren't hard to draw a prominent conclusion that the ingested rate of tissues to HSYA, NAG, and pCA was quicker than other analytes in GHI. We inferred maybe the larger concentration difference between both sides of the cytomembrane caused by the higher content of these three ingredients in GHI made a stupendous contribution to their more rapid intake by tissues.

CL, one of PK parameters, reflected the elimination rate of drugs in the organism. We discovered that the value of CL_2 of all analytes was larger than CL_1, declaring that the elimination speed of all ingredients in the peripheral compartment was quicker than in the central compartment. After comparing the alteration of CL_1 and CL_2 of all compounds with the increase in the dose of GHI, we readily divided all components into three groups. The first kind was ingredients with an enlargement of both CL_1 and CL_2, including NAG and pCA. We conjectured the acceleration of the clearance of these two compounds due to their strong water-solubility and low molecular mass. The second kind was compounds with a diminution of both CL_1 and CL_2, containing HYP and K-3-R. The third was constituents (i.e., HSYA, CGA, K-3-G, and RT) with a decrease of CL_1 and an increase of CL_2. We believed the cause for the decline in the clearance of these six compositions ought to comprehensively consider multiple factors, such as their content, polarity, molecular weight, and the binding rate of plasma protein.

Based on PK/PD study, two machine learning approaches, principal component analysis (PCA) and back propagation neural network (BPNN), have been adopted to investigate the contribution of ingredients in drugs to diverse effects in previous studies [30,31]. Although PCA, BPNN, and PLSR all were able to achieve that intention, compared to PLSR, PCA and BPNN exhibited a modicum of flaws. The principle of PLSR was slightly different from that of PCA, that is PLSR aimed to search for direction with both high square error and high correlation with response variables, but PCA only

paid attention to the former [32,33]. We inferred that the reason why PLSR attained both the positive−negative correlation and contribution rate, but PCA only acquired the latter may be associated with that difference. Due to the complexity of model and the small sample size, the application of BPNN may result in over-fitting [34]. The adoption of cross-validation in PLSR effectively avoided the over-fitting, meanwhile, PLSR may exhibit better applicability to the research with a modest amount of sample [35,36]. In this research, we considered each myocardial enzyme as the independent variable and all analytes as the dependent variable to establish PLSR analysis. The weighted coefficients of all PLSR equations demonstrated NAG, HSYA, CGA, and pCA were positively correlated with the decline of all cardiac enzymes, declaring these four compounds may serve as the active ingredients of GHI in treating MI/R injury.

GHI effectively decreased the level of one enzyme, CK-MB, closely related to energy metabolism in the myocardium [37]. NAG, one ingredient with the maximum content in GHI, was further transformed into glutamate in the organism, while glutamate played a significant role in the energy balance of H9c2 after hypoxia/reoxygenation [38,39]. We speculated that adjusting energy metabolism may be one principal therapeutic mechanism of GHI on MI/R injury. In previous studies, IMA was widely regarded as a biomarker to assess both oxidative stress and myocardial ischemia, whose level was also declined by GHI in the current study [40−42]. HSYA is a compound with the second content in GHI, whose brilliant antioxidant effect when mitigating MI/R injury has already been verified in antecedent research [43]. Hence, we believed that the antioxidant effect, as the other momentous mechanism of GHI on protecting the myocardium from damage, was undisputed. Furthermore, the generation of IMA may induce the anomalous concentration of cellular transition elements, such as iron ions and copper ions, possibly further leading to ferroptosis and cuproptosis. Previous research proved HSYA possessed a regulatory effect to ferroptosis in rats' pheochromocytoma cell line (PC12), but there were no studies about HSYA adjusting ferroptosis, one monumental mechanism of MI/R injury [44,45]. We thought the research on mechanisms of GHI based on ferroptosis and cuproptosis in treating MI/R injury was also condignly pondered. cTn I was one calcium-dependent subunit of cardiac troponin, whose level was equally diminished by GHI in our study [46,47]. Combining the corroboration that HSYA, CGA, and

*p*CA were able to adjust the level of intracellular calcium, we inferred that the balance of cellular calcium ions probably was another mechanism of GHI in the therapy of MI/R injury because calcium overload also is one pivotal pathogenesis [48−51]. α-HBDH has been affirmed to participate in glycolysis to generate numerous lactic acids, resulting in acidosis of the myocardium [26,52]. In our current research, the level of α-HBDH was also descended by GHI. Previous studies demonstrated that polyphenols, such as CGA and *p*CA, effectively inhibited glycolysis [53−55]. We inferred that the inhibition of glycolysis to avoid engendering superfluous lactic acid to prevent acidosis of the organism may also be one mechanism of GHI in curing MI/R injury. On the whole, the cardioprotective effect of GHI tentatively behaved in the following four aspects, adjusting energy metabolism, inhibiting oxidative stress reaction, regulating calcium ions, and suppressing glycolysis.

PK/PD studies deduced the concentration that produced effects, optimized the administered dose, as well as provided a scientific basis for the optimum administration regimen via investigating the three−dimensional relationship of concentration-effect-time [56]. Owing to the cardioprotective effect of GHI *in vivo* and *in vitro* has been affirmed in our previous research, we proceeded with PK/PD studies to supply guidelines for the clinical medication of GHI in treating MI/R injury [21]. In the present study, analytes with a negative coefficient in PLSR equations and four cardiac enzymes (i.e., CK-MB, cTn I, IMA, and α-HBDH) were respectively regarded as PK and PD indicators to fit PK/PD model. After comparing the variation of parameters in PK/PD equations when the dose of GHI was magnified, we discovered that E_{max} and ED_{50} of most ingredients raised when the dose of GHI was magnified. The increase in E_{max} represented GHI with a high dose generated a better intrinsic activity, which proclaimed its curative effect on four myocardial enzymes was optimum. The ascension in ED_{50} stood for that the components in GHI with a high dose possessed a worse affinity with receptors, which may be caused by the saturation of receptors.

Taken together, the PK characteristics and PK/PD models of analytes and biomarkers in three concentrations of GHI were triumphantly established and compared. All analytes in GHI possessed a feature of rapid distribution and slow elimination, and their distributed and eliminated position was dominantly located in the peripheral compartment. With the enhancement of the dose of GHI, the ingredients were only filled in the central compartment if the peripheral compartment was replete. Meanwhile, GHI with a high dose generated the optimum intrinsic activity, but the affinity of compounds with receptors was the worst, which may be caused by the saturation of receptors. Among the eight analytes, NAG, HSYA, CGA, and *p*CA exhibited more excellent cardioprotection, which probably served as the pharmacodynamic substance basis of GHI on the remedy of MI/R injury.

Conflicts of interest

All authors appeared in this paper avow none of any conflicts of interest.

Data availability statement

The correspondence author is responsible to furnish all primordial data applied to bear our figures and conclusions, as well as the chemical standard and drug specimen used in this research.

Acknowledgements

Appendix

Supplementary Table 1. Linear regression equations for the quantification of analytes.

Analytes	Regression equations	R^2	Linear ranges (ng/mL)
Chlorogenic acid	y = 4.25772x+0.03728	0.99642	0.1−5000
Hydroxysafflor yellow A	y = 0.22021x+0.02726	0.99739	1~10000
Hyperoside	$y = 4.04239x - 4.37059 \times 10^{-5}$	0.99593	0.1−1000
Kaempferol-3-O-glucoside	$y = 5.65151x + 7.439 \times 10^{-4}$	0.99651	0.1−1000
Kaempferol-3-O-rutinoside	y = 3.44678x+0.00290	0.99381	0.1−10000
N-acetyl-L-glutamine	y = 0.62787x+0.04163	0.99437	1~10000
p-Coumaric acid	y = 0.82290x+0.01107	0.99843	0.1−10000
Rutin	y = 3.96159x+0.00575	0.99665	0.1−1000

Supplementary Table 2. Results for intra-precision, inter-precision, intra-accuracy, and inter-accuracy of analytes (n = 6).

Analytes	Concentrations (ng/mL)	Precision (RSD)		Accuracy (RE)	
		Intra-precision	Inter-precision	Intra-accuracy	Inter-accuracy
Chlorogenic acid	5	2.99%	4.55%	−3.03%	−5.43%
	50	3.86%	4.09%	5.08%	4.59%
	500	3.33%	3.92%	−7.86%	−6.04%
Hydroxysafflor yellow A	5	3.55%	7.48%	8.48%	3.08%
	50	5.87%	4.89%	3.61%	3.57%
	500	4.51%	3.17%	−9.49%	−9.95%
Hyperoside	5	3.21%	3.77%	6.07%	10.42%
	50	2.57%	4.98%	8.14%	4.87%
	500	2.35%	3.31%	−6.96%	−7.41%
Kaempferol-3-O-glucoside	5	2.19%	2.42%	2.92%	4.81%
	50	1.63%	2.18%	5.98%	4.41%
	500	2.49%	3.33%	−9.48%	−8.02%
Kaempferol-3-O-rutinoside	5	7.45%	5.67%	0.19%	2.70%
	50	2.31%	2.86%	8.97%	7.69%
	500	3.71%	4.26%	−8.31%	−5.51%
N-acetyl-L-glutamine	5	2.63%	3.26%	5.13%	7.35%
	50	4.53%	4.68%	1.91%	4.29%
	500	0.97%	2.08%	10.98%	9.53%
p-Coumaric acid	5	1.51%	5.03%	1.01%	3.18%
	50	3.53%	3.62%	5.41%	6.99%
	500	3.95%	4.35%	3.76%	1.86%
Rutin	5	3.88%	3.92%	−11.51%	−8.28%
	50	2.03%	3.07%	5.37%	6.72%
	500	4.81%	4.17%	−0.23%	−1.03%

Supplementary Table 3. Results for matrix effect of analytes (n = 6).

Analytes	Concentration (ng/mL)	Matrix effect	
		(Mean ± SD)%	RSD%
Chlorogenic acid	5	97.59 ± 3.65	3.74
	50	98.37 ± 1.70	1.73
	500	103.42 ± 5.28	5.10
Hydroxysafflor yellow A	5	100.86 ± 0.88	0.88
	50	98.95 ± 4.01	4.06
	500	102.96 ± 3.59	3.49
Hyperoside	5	100.52 ± 5.01	4.98
	50	100.97 ± 2.67	2.64
	500	101.35 ± 3.68	3.64
Kaempferol-3-O-glucoside	5	96.12 ± 2.14	2.23
	50	100.37 ± 3.73	3.71
	500	99.40 ± 4.08	4.10
Kaempferol-3-O-rutinoside	5	109.14 ± 1.28	1.17
	50	100.85 ± 2.00	1.98
	500	99.99 ± 5.80	5.80
N-acetyl-L-glutamine	5	101.21 ± 1.80	1.78
	50	100.81 ± 2.33	2.31
	500	99.21 ± 4.21	4.24
p-Coumaric acid	5	99.56 ± 6.78	6.81
	50	102.13 ± 2.70	2.64
	500	97.67 ± 3.88	3.97
Rutin	5	101.12 ± 5.03	4.97
	50	100.57 ± 2.40	2.38
	500	98.90 ± 4.86	4.91

Supplementary Table 4. Results of freeze-thaw stability (three times) of all analytes (n = 6).

Analytes	Concentration (ng/mL)	Mean ± SD	RSD	RE
Chlorogenic acid	5	4.527 ± 0.130	2.86%	−9.46%
	50	50.717 ± 1.737	3.42%	1.43%
	500	483.647 ± 9.298	1.92%	−3.27%
Hydroxysafflor yellow A	5	5.115 ± 0.341	6.66%	2.30%
	50	50.550 ± 1.276	2.52%	1.10%
	500	508.052 ± 21.065	4.15%	1.61%
Hyperoside	5	5.384 ± 0.142	2.64%	7.69%
	50	51.911 ± 1.743	3.36%	3.82%
	500	488.61 ± 16.242	3.33%	−2.37%
Kaempferol-3-O-glucoside	5	5.390 ± 0.067	1.24%	7.80%
	50	53.303 ± 1.079	2.02%	6.61%
	500	524.815 ± 22.328	4.25%	4.96%
Kaempferol-3-O-rutinoside	5	5.479 ± 0.134	2.45%	9.58%
	50	52.642 ± 0.771	1.46%	5.28%
	500	539.455 ± 23.696	4.39%	7.89%
N-acetyl-L-glutamine	5	5.109 ± 0.257	5.03%	2.18%
	50	50.906 ± 3.522	6.92%	1.81%
	500	527.696 ± 15.640	2.96%	5.54%
p-Coumaric acid	5	4.891 ± 0.196	4.01%	−2.18%
	50	53.579 ± 2.574	4.80%	7.16%
	500	510.543 ± 9.094	1.78%	2.11%
Rutin	5	5.067 ± 0.211	4.17%	1.35%
	50	53.579 ± 2.574	4.80%	7.16%
	500	548.234 ± 7.459	1.36%	9.65%

Supplementary Table 5. Results of auto-sampler stability of all analytes (n = 6).

Analytes	Concentration (ng/mL)	Mean ± SD	RSD	RE
Chlorogenic acid	5	5.156 ± 0.213	4.14%	3.12%
	50	49.668 ± 0.637	1.28%	−0.66%
	500	494.325 ± 9.584	1.94%	−1.13%
Hydroxysafflor yellow A	5	4.587 ± 0.345	7.53%	−8.26%
	50	51.730 ± 2.499	4.83%	3.46%
	500	445.193 ± 18.692	4.20%	−10.96%
Hyperoside	5	5.605 ± 0.106	1.90%	12.10%
	50	49.993 ± 1.567	3.13%	−0.01%
	500	496.332 ± 14.309	2.88%	−0.74%
Kaempferol-3-O-glucoside	5	4.871 ± 0.096	1.96%	−2.57%
	50	53.220 ± 0.849	1.59%	6.44%
	500	503.803 ± 13.019	2.58%	0.76%
Kaempferol-3-O-rutinoside	5	5.564 ± 0.086	1.55%	11.28%
	50	53.665 ± 1.318	2.46%	7.33%
	500	466.409 ± 9.188	1.97%	−6.72%
N-acetyl-L-glutamine	5	5.156 ± 0.213	4.14%	3.12%
	50	53.515 ± 1.230	2.30%	7.03%
	500	475.086 ± 11.904	2.51%	−4.98%
p-Coumaric acid	5	4.911 ± 0.361	7.35%	−1.78%
	50	49.060 ± 2.742	5.59%	−1.88%
	500	464.716 ± 15.671	3.37%	−7.06%
Rutin	5	5.127 ± 0.136	2.65%	2.55%
	50	53.819 ± 1.185	2.20%	7.64%
	500	466.02 ± 13.77	2.95%	−6.80%

Supplementary Table 6. Results of long-term stability of all analytes (n = 6).

Analytes	Concentration (ng/mL)	Mean ± SD	RSD	RE
Chlorogenic acid	5	4.906 ± 0.166	3.38%	−1.87%
	50	51.665 ± 1.135	2.20%	3.33%
	500	486.234 ± 6.641	1.37%	−2.75%
Hydroxysafflor yellow A	5	4.926 ± 0.445	9.02%	−1.47%
	50	52.330 ± 3.583	6.85%	4.66%
	500	459.868 ± 17.911	3.89%	−8.03%
Hyperoside	5	5.524 ± 0.158	2.87%	10.49%
	50	51.942 ± 2.597	5.00%	3.88%
	500	446.621 ± 9.428	2.11%	−10.68%
Kaempferol-3-O-glucoside	5	5.384 ± 0.124	2.31%	7.69%
	50	53.701 ± 1.321	2.46%	7.40%
	500	447.438 ± 13.203	2.95%	−10.51%
Kaempferol-3-O-rutinoside	5	5.381 ± 0.118	2.20%	7.63%
	50	54.438 ± 0.739	1.36%	8.88%
	500	449.835 ± 15.067	3.35%	−10.03%
N-acetyl-L-glutamine	5	5.314 ± 0.334	6.29%	6.29%
	50	50.765 ± 3.523	6.94%	1.53%
	500	482.449 ± 8.508	1.76%	−3.51%
p-Coumaric acid	5	5.332 ± 0.157	2.95%	6.44%
	50	51.732 ± 2.278	4.40%	3.46%
	500	456.425 ± 12.555	2.75%	−8.72%
Rutin	5	5.034 ± 0.171	3.40%	0.69%
	50	51.383 ± 1.524	2.97%	2.77%
	500	451.281 ± 5.824	1.29%	−9.74%

Supplementary Table 7. Results of dilution integrity of N-acetyl-L-glutamine and hydroxysafflor yellow A (n = 6).

| Analytes	Dilution factor	Mean ± SD	RSD	RE
Hydroxysafflor yellow A	50-fold	9827.441 ± 234.840	2.39%	−1.73%
	200-fold	9615.733 ± 202.626	2.11%	−3.84%
N-acetyl-L-glutamine	50-fold	9538.954 ± 96.996	1.02%	−4.61%
	200-fold	9390.746 ± 173.661	1.85%	−6.09%
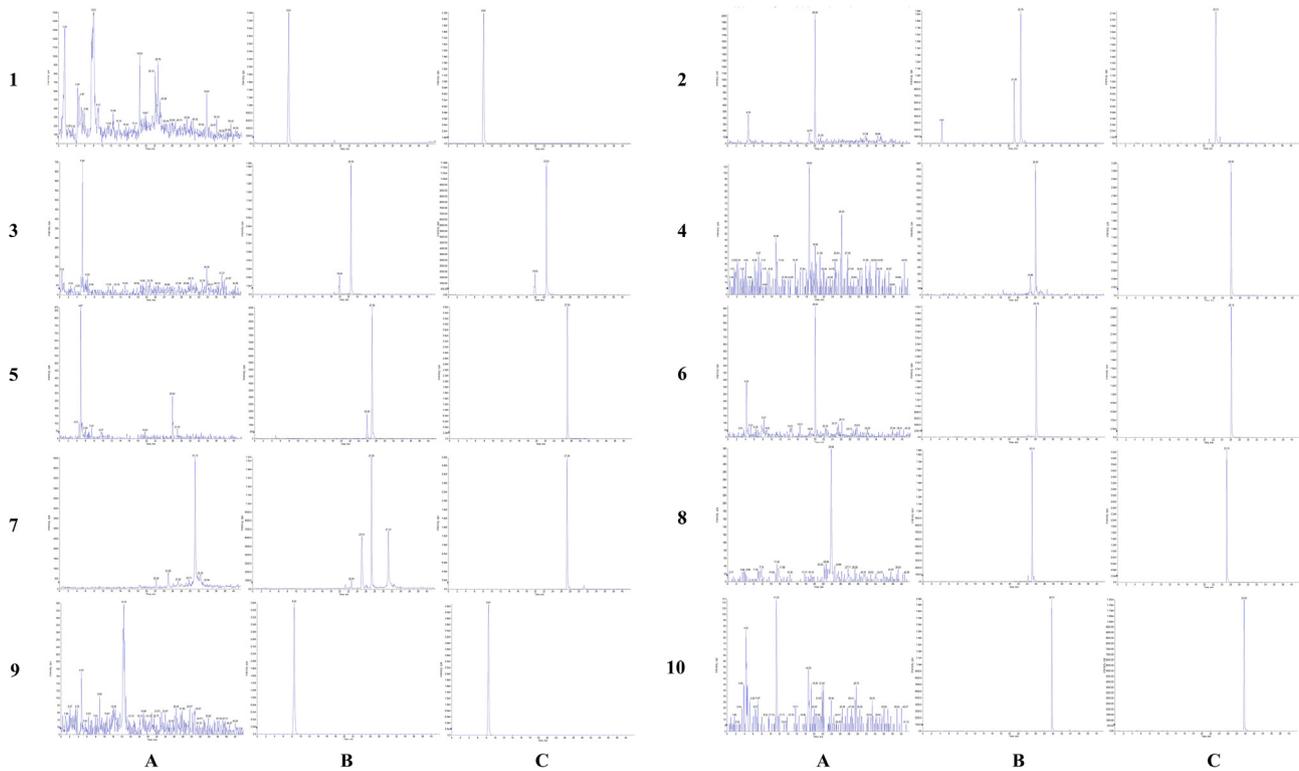
Fig. S1. The retention time of eight analytes and two ISs, i.e., N-acetyl-L-glutamine (1), chlorogenic acid (2), hydroxysafflor yellow A (3), hyperoside (4), kaempferol-3-O-glucoside (5), kaempferol-3-O-rutinoside (6), p-coumaric acid (7), rutin (8), N-carbamoyl-L-glutamate (9), and icariin (10), in the blank plasma (A), the drug-contained plasma spiked with ISs (B), and the mixed standard solution added with ISs (C).
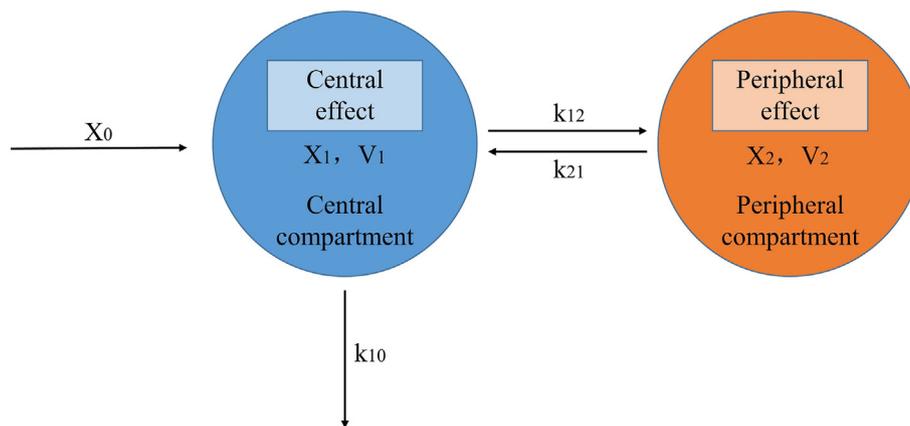

Fig. S2. The PK/PD model diagram of the present study.

References

[1] Boateng Sanborn T. Acute myocardial infarction. Dis Mon 2013;59:83—96. https://doi.org/10.1016/j.disamonth.2012.12.004.

[2] Rentrop Pblanke H. Percutaneous transluminal coronary artery recanalization in evolving myocardial infarction. Cardiovasc Intervent Radiol 1982;5:194—6. https://doi.org/10.1007/bf02552309.

[3] Tehrani BN, Basir MB, Kapur NK. Acute myocardial infarction and cardiogenic shock: should we unload the ventricle before percutaneous coronary intervention? Prog Cardiovasc Dis 2020;63:607—22. https://doi.org/10.1016/j.pcad.2020.09.001.

[4] Ye J, Lu S, Wang M, Ge W, Liu H, Qi Y, et al. Hydroxysafflor yellow A protects against myocardial ischemia/reperfusion injury via suppressing NLRP3 inflammasome and activating autophagy. Front Pharmacol 2020;11:1170. https://doi.org/10.3389/fphar.2020.01170.

[5] Min Jwei C. Hydroxysafflor yellow A cardioprotection in ischemia-reperfusion (I/R) injury mainly via Akt/hexokinase II independent of ERK/GSK-3β pathway. Biomed Pharmacother 2017;87:419—26. https://doi.org/10.1016/j.biopha.2016.12.113.

[6] Lu QY, Ma JQ, Duan YY, Sun Y, Yu S, Li B, et al. Carthamin yellow protects the heart against ischemia/reperfusion injury with reduced reactive oxygen species release and inflammatory response. J Cardiovasc Pharmacol 2019;74:228—34. https://doi.org/10.1097/fjc.0000000000000710.

[7] Xiao X, Lan W, Zhao Y, Li R, Liu Y, Liu J, et al. In vivo pharmacokinetic and pharmacodynamic (PK/PD) modeling and establishment of the PK/PD cutoff of florfenicol against pasteurella multocida in ducks. Front Microbiol 2020;11:616685. https://doi.org/10.3389/fmicb.2020.616685.

[8] Chowdhury EA, Meno-Tetang G, Chang HY, Wu S, Huang HW, Jamier T, et al. Current progress and limitations of AAV mediated delivery of protein therapeutic genes and the importance of developing quantitative pharmacokinetic/pharmacodynamic (PK/PD) models. Adv Drug Deliv Rev 2021;170:214—37. https://doi.org/10.1016/j.addr.2021.01.017.

[9] Zhang X, Lv S, Zhang W, Jia Q, Wang L, Ding Y, et al. Shenmai injection improves doxorubicin cardiotoxicity via miR-30a/Beclin 1. Biomed Pharmacother 2021;139:111582. https://doi.org/10.1016/j.biopha.2021.111582.

[10] Chen Q, Wan J, Zhang Y, He Y, Bao Y, Yu L, et al. Pharmacokinetic-pharmacodynamic modeling analysis for hydroxysafflor yellow A-calycosin in compatibility in normal and cerebral ischemic rats: a comparative study. Biomed Pharmacother 2022;150:112950. https://doi.org/10.1016/j.biopha.2022.112950.

[11] Yu Y, Zhu Z, Xie M, Deng L, Xie X, Zhang M. Investigation on the Q-markers of Bushen Huoxue Prescriptions for DR treatment based on chemometric methods and spectrum-effect relationship. J Ethnopharmacol 2022;285:114800. https://doi.org/10.1016/j.jep.2021.114800.

[12] Qiu Q, Jiang L, Huang C, Yu L, Zhen D, Ye M, et al. Study on the spectrum-effect correlation of anti-inflammatory active extract of Sauropus spatulifolius beille. J Anal Methods Chem 2022:5646546. https://doi.org/10.1155/2022/5646546.

[13] Nijat D, Lu CF, Lu JJ, Abdulla R, Hasan A, Aidarhan N, et al. Spectrum-effect relationship between UPLC fingerprints and antidiabetic and antioxidant activities of Rosa rugosa. J Chromatogr B Analyt Technol Biomed Life Sci 2021;1179:122843. https://doi.org/10.1016/j.jchromb.2021.122843.

[14] Fan J, Ma J, Xia N, Sun L, Li B, Liu H. Clinical value of combined detection of CK-mb, MYO, cTnI and plasma NT-proBNP in diagnosis of acute myocardial infarction. Clin Lab 2017;63:427—33. https://doi.org/10.7754/Clin.Lab.2016.160533.

[15] Shevtsova A, Gordiienko I, Tkachenko V, Ushakova G. Ischemia-modified albumin: origins and clinical implications. Dis Markers 2021:9945424. https://doi.org/10.1155/2021/9945424.

[16] Shi W, Tang G, Zhou X, Ye Y. Appraising the accuracy of ischaemia-modified albumin in diagnosing stroke: a systematic review and meta-analysis. Cerebrovasc Dis 2021;50:365—70. https://doi.org/10.1159/000514382.

[17] Kõncõ MF, Kasap B, Sivaslõoǧlu AA. Ischemia-modified albumin in gynecology. Biomark Med 2021;15:455—62. https://doi.org/10.2217/bmm-2020-0616.

[18] Gallacher PJ, Miller-Hodges E, Shah ASV, Farrah TE, Halbesma N, Blackmur JP, et al. High-sensitivity cardiac troponin and the diagnosis of myocardial infarction in patients with kidney impairment. Kidney Int 2022;102:149—59. https://doi.org/10.1016/j.kint.2022.02.019.

[19] Antman EM. The introduction and clinical use of cardiac-specific troponin assays. Clin Pharmacol Ther 2018;103:31—3. https://doi.org/10.1002/cpt.773.

[20] Bai Z, Ma Y, Shi Z, Li T, Hu S, Shi B. Nomogram for the prediction of intrahospital mortality risk of patients with ST-segment elevation myocardial infarction complicated with hyperuricemia: a multicenter retrospective study. Ther Clin Risk Manag 2021;17:863—75. https://doi.org/10.2147/tcrm.S320533.

[21] Chen H, Zhou H, Yang J, Wan H, He Y. Guhong injection mitigates myocardial ischemia/reperfusion injury by activating GST P to inhibit ASK1-JNK/p38 pathway. Phytomedicine 2023;109:154603. https://doi.org/10.1016/j.phymed.2022.154603.

[22] Yu L, Wan HF, Li C, Yang JH, Zhou HF, Wan HT, et al. Pharmacokinetics of active components from guhong injection in normal and pathological rat models of cerebral ischemia: a comparative study. Front Pharmacol 2018;9:493. https://doi.org/10.3389/fphar.2018.00493.

[23] Yu L, Zhang Y, Zhao X, Wan H, He Y, Jin W. Guhong injection alleviates cerebral ischemia-reperfusion injury via the PKC/HIF-1α pathway in rats. Front Pharmacol 2021;12:716121. https://doi.org/10.3389/fphar.2021.716121.

[24] Wiedemair Vhuck CW. Evaluation of the performance of three hand-held near-infrared spectrometer through investigation of total antioxidant capacity in gluten-free grains. Talanta 2018;189:233—40. https://doi.org/10.1016/j.talanta.2018.06.056.

[25] Singh S, Gumbo T, Boorgula GD, Shankar P, Heysell SK, Srivastava S. Omadacycline pharmacokinetics/pharmacodynamics in the hollow fiber system model and potential combination regimen for short course treatment of Mycobacterium kansasii pulmonary disease. Antimicrob Agents Chemother 2022;66:e0068722. https://doi.org/10.1128/aac.00687-22.

[26] Wang ZW, Liu C, Zhang AH, Yan GL, Sun H, Han Y, et al. Discovery of Q-markers of wenxin formula based on a chinmedomics strategy. J Ethnopharmacol 2022;298:115576. https://doi.org/10.1016/j.jep.2022.115576.

[27] Haughan JE, Missanelli JR, You Y, Stefanovski D, Soma LR, Robinson MA. Pharmacokinetics of glaucine after intravenous and oral administrations and detection of systemic aporphine alkaloids after ingestion of tulip poplar shavings in horses. J Vet Pharmacol Ther 2022;45:273—82. https://doi.org/10.1111/jvp.13057.

[28] Slimano F, Djerada Z, Bouchene S, Van Gulick L, Brassart-Pasco S, Dukic S. First plasma and tissue pharmacokinetic study of the YSNSG cyclopeptide, a new integrin antagonist, using microdialysis. Eur J Pharm Sci 2017;105:178—87. https://doi.org/10.1016/j.ejps.2017.05.016.

[29] Guan H, Lin Q, Ma C, Ju Z, Wang C. Metabolic profiling and pharmacokinetic studies of sinapine thiocyanate by UHPLC-Q/TOF-MS and UHPLC-MS/MS. J Pharm Biomed Anal 2022;207:114431. https://doi.org/10.1016/j.jpba.2021.114431.

[30] Yeqing C, Xinsheng F, Liping Z, Fangyuan H, Pengli W. Screening and evaluation of quality markers from Shuangshen Pingfei formula for idiopathic pulmonary fibrosis using network pharmacology and pharmacodynamic, phytochemical, and pharmacokinetic analyses. Phytomedicine 2022;100:154040. https://doi.org/10.1016/j.phymed.2022.154040.

[31] Chen YC, Cao WW, Cao Y, Zhang L, Chang BB, Yang WL, et al. Using neural networks to determine the contribution of danshensu to its multiple cardiovascular activities in acute myocardial infarction rats. J Ethnopharmacol 2011;138: 126−34. https://doi.org/10.1016/j.jep.2011.08.069.

[32] Stacey P, Clegg F, Sammon C. Multicomponent measurement of respirable quartz, kaolinite and coal dust using fourier transform infrared spectroscopy (FTIR): a comparison between partial least squares and principal component regressions. Ann Work Expo Health 2022;66:644−55. https://doi.org/10.1093/annweh/wxab081.

[33] Liu C, Zhang X, Nguyen TT, Liu J, Wu T, Lee E, et al. Partial least squares regression and principal component analysis: similarity and differences between two popular variable reduction approaches. Gen Psychiatr 2022;35:e100662. https://doi.org/10.1136/gpsych-2021-100662.

[34] Pan S, Zhou J, Zhou S, Huang Z, Meng J. Pharmacokinetic-pharmacodynamic modeling for Moutan Cortex/Moutan Cortex charcoal and the contributions of the chemical component using support vector regression with particle swarm optimization. RSC Adv 2020;10:24454−62. https://doi.org/10.1039/d0ra04111d.

[35] Huang C, Du J, Nie B, Yu R, Xiong W, Zeng Q. Feature selection method based on partial least squares and analysis of traditional Chinese medicine data. Comput Math Methods Med 2019;9580126. https://doi.org/10.1155/2019/9580126.

[36] Bertrand Fmaumy-Bertrand M. Fitting and cross-validating cox models to censored big data with missing values using extensions of partial least squares regression models. Front Big Data 2021;4:684794. https://doi.org/10.3389/fdata.2021.684794.

[37] Kurapati Rsoos MP, CPK MB. StatPearls. Treasure Island (FL: StatPearls Publishing Copyright © 2022, StatPearls Publishing LLC; 2022.

[38] Maiolino M, Castaldo P, Lariccia V, Piccirillo S, Amoroso S, Magi S. Essential role of the Na(+)-Ca2(+) exchanger (NCX) in glutamate-enhanced cell survival in cardiac cells exposed to hypoxia/reoxygenation. Sci Rep 2017;7:13073. https://doi.org/10.1038/s41598-017-13478-x.

[39] Xu S, Li C, Zhou H, Yu L, Deng L, Zhu J, et al. A study on acetylglutamine pharmacokinetics in rat blood and brain based on liquid chromatography-tandem mass spectrometry and microdialysis technique. Front Pharmacol 2020;11:508. https://doi.org/10.3389/fphar.2020.00508.

[40] Aladağ N, Asoğlu R, Ozdemir M, Asoğlu E, Derin AR, Demir C, et al. Oxidants and antioxidants in myocardial infarction (MI): investigation of ischemia modified albumin, malondialdehyde, superoxide dismutase and catalase in individuals diagnosed with ST elevated myocardial infarction (STEMI) and non-STEMI (NSTEMI). J Med Biochem 2021;40: 286−94. https://doi.org/10.5937/jomb0-28879.

[41] Tampa M, Mitran CI, Mitran MI, Amuzescu A, Matei C, Georgescu SR. Ischemia-modified albumin-A potential new marker of oxidative stress in dermatological diseases. Medicina (Kaunas) 2022;58. https://doi.org/10.3390/medicina58050669.

[42] Xiao LL, Zhang F, Zhao YL, Zhang LJ, Xie ZY, Huang KZ, et al. Using advanced oxidation protein products and ischaemia-modified albumin to monitor oxidative stress levels in patients with drug-induced liver injury. Sci Rep 2020;10:18128. https://doi.org/10.1038/s41598-020-75141-2.

[43] Zhou D, Ding T, Ni B, Jing Y, Liu S. Hydroxysafflor Yellow A mitigated myocardial ischemia/reperfusion injury by inhibiting the activation of the JAK2/STAT1 pathway. Int J Mol Med 2019;44:405−16. https://doi.org/10.3892/ijmm.2019.4230.

[44] Chen G, Li C, Zhang L, Yang J, Meng H, Wan H, et al. Hydroxysafflor yellow A and anhydrosafflor yellow B alleviate ferroptosis and parthanatos in PC12 cells injured by OGD/R. Free Radic Biol Med 2022;179:1−10. https://doi.org/10.1016/j.freeradbiomed.2021.12.262.

[45] Zhao WK, Zhou Y, Xu TT, Wu Q. Ferroptosis: opportunities and challenges in myocardial ischemia-reperfusion injury. Oxid Med Cell Longev 2021:9929687. https://doi.org/10.1155/2021/9929687.

[46] Park KC, Gaze DC, Collinson PO, Marber MS. Cardiac troponins: from myocardial infarction to chronic disease. Cardiovasc Res 2017;113:1708−18. https://doi.org/10.1093/cvr/cvx183.

[47] Hantz ERLindert S. Computational exploration and characterization of potential calcium sensitizing mutations in cardiac troponin C. J Chem Inf Model 2022;62:6201−8. https://doi.org/10.1021/acs.jcim.2c01132.

[48] Ye J, Wang R, Wang M, Fu J, Zhang Q, Sun G, et al. Hydroxysafflor yellow A ameliorates myocardial ischemia/reperfusion injury by suppressing calcium overload and apoptosis. Oxid Med Cell Longev 2021:6643615. https://doi.org/10.1155/2021/6643615.

[49] Jung HJ, Im SS, Song DK, Bae JH. Effects of chlorogenic acid on intracellular calcium regulation in lysophosphatidylcholine-treated endothelial cells. BMB Rep 2017;50:323−8. https://doi.org/10.5483/bmbrep.2017.50.6.182.

[50] Chacko SM, Nevin KG, Dhanyakrishnan R, Kumar BP. Protective effect of p-coumaric acid against doxorubicin induced toxicity in H9c2 cardiomyoblast cell lines. Toxicol Rep 2015;2:1213−21. https://doi.org/10.1016/j.toxrep.2015.08.002.

[51] Valikeserlis I, Athanasiou AA, Stakos D. Cellular mechanisms and pathways in myocardial reperfusion injury. Coron Artery Dis 2021;32:567−77. https://doi.org/10.1097/mca.0000000000000997.

[52] Lu M, Jia M, Wang Q, Guo Y, Li C, Ren B, et al. The electrogenic sodium bicarbonate cotransporter and its roles in the myocardial ischemia-reperfusion induced cardiac diseases. Life Sci 2021;270:119153. https://doi.org/10.1016/j.lfs.2021.119153.

[53] Zhou Y, Ruan Z, Zhou L, Shu X, Sun X, Mi S, et al. Chlorogenic acid ameliorates endotoxin-induced liver injury by promoting mitochondrial oxidative phosphorylation. Biochem Biophys Res Commun 2016;469:1083−9. https://doi.org/10.1016/j.bbrc.2015.12.094.

[54] Aslan E, Guler C, Adem S. In vitro effects of some flavonoids and phenolic acids on human pyruvate kinase isoenzyme M2. J Enzyme Inhib Med Chem 2016;31:314−7. https://doi.org/10.3109/14756366.2015.1022173.

[55] Martel F, Guedes M, Keating E. Effect of polyphenols on glucose and lactate transport by breast cancer cells. Breast Cancer Res Treat 2016;157:1−11. https://doi.org/10.1007/s10549-016-3794-z.

[56] Song F, Zheng X, Wang Y, Chow SC, Sun H. Innovative design and analysis for PK/PD biosimilar bridging studies with multiple references. AAPS J 2021;24:3. https://doi.org/10.1208/s12248-021-00658-x.